Neurobiology of Disease

SIRT3 Haploinsufficiency Aggravates Loss of GABAergic Interneurons and Neuronal Network Hyperexcitability in an Alzheimer's Disease Model

Aiwu Cheng,[1,5]* Jing Wang,[1,2]* Nathaniel Ghena,[1] Qijin Zhao,[1] Isabella Perone,[1,5] Todd M. King,[3] Richard L. Veech,[3] Myriam Gorospe,[5] Ruiqian Wan,[1] and Mark P. Mattson[1,4]

[1]Laboratory of Neurosciences, National Institute on Aging Intramural Research Program, National Institutes of Health, Baltimore, Maryland 21224, [2]Department of Integrative Medicine and Neurobiology, Institutes of Brain Science, Shanghai Medical College, Fudan University, Shanghai, China 200030, [3]Laboratory of Metabolic Control, National Institute on Alcohol Abuse and Alcoholism, National Institutes of Health, Bethesda, Maryland 20892, [4]Department of Neuroscience, Johns Hopkins University School Medicine, Baltimore, Maryland 21205, and [5]Laboratory of Genetics and Genomics, National Institute on Aging Intramural Research Program, National Institutes of Health, Baltimore, Maryland 21224

Impaired mitochondrial function and aberrant neuronal network activity are believed to be early events in the pathogenesis of Alzheimer's disease (AD), but how mitochondrial alterations contribute to aberrant activity in neuronal circuits is unknown. In this study, we examined the function of mitochondrial protein deacetylase sirtuin 3 (SIRT3) in the pathogenesis of AD. Compared with AppPs1 mice, Sirt3-haploinsufficient AppPs1 mice (Sirt3 $^{+/-}$AppPs1) exhibit early epileptiform EEG activity and seizure. Both male and female Sirt3 $^{+/-}$AppPs1 mice were observed to die prematurely before 5 months of age. When comparing male mice among different genotypes, Sirt3 haploinsufficiency renders GABAergic interneurons in the cerebral cortex vulnerable to degeneration and associated neuronal network hyperexcitability. Feeding Sirt3 $^{+/-}$AppPs1 AD mice with a ketone ester-rich diet increases SIRT3 expression and prevents seizure-related death and the degeneration of GABAergic neurons, indicating that the aggravated GABAergic neuron loss and neuronal network hyperexcitability in Sirt3 $^{+/-}$AppPs1 mice are caused by SIRT3 reduction and can be rescued by increase of SIRT3 expression. Consistent with a protective role in AD, SIRT3 levels are reduced in association with cerebral cortical Aβ pathology in AD patients. In summary, SIRT3 preserves GABAergic interneurons and protects cerebral circuits against hyperexcitability, and this neuroprotective mechanism can be bolstered by dietary ketone esters.

Key words: Alzheimer disease; GABAergic; hyperexcitability; mitochondria; seizure; telemetry

Significance Statement

GABAergic neurons provide the main inhibitory control of neuronal activity in the brain. By preserving mitochondrial function, SIRT3 protects parvalbumin and calretinin interneurons against Aβ-associated dysfunction and degeneration in AppPs1 Alzheimer's disease mice, thus restraining neuronal network hyperactivity. The neuronal network dysfunction that occurs in Alzheimer's disease can be partially reversed by physiological, dietary, and pharmacological interventions to increase SIRT3 expression and enhance the functionality of GABAergic interneurons.

Introduction

The clinical diagnosis of probable Alzheimer's disease (AD) is based on the progressive deterioration of short-term memory and the presence of amyloid β-peptide (Aβ) plaques and degenerated neurons exhibiting tau tangles. Aβ pathology, however, is not always sufficient to cause synaptic dysfunction and neuronal degeneration as some elderly individuals exhibit abundant Aβ plaques but remain cognitively normal, and many transgenic AD mouse models exhibit robust Aβ plaque pathology and moderate cognitive impairment but with little or no neuronal death (Ashe

Received June 20, 2019; revised Sept. 26, 2019; accepted Nov. 5, 2019.

Author contributions: A.C. and M.P.M. designed research; A.C., J.W., N.G., Q.Z., I.P., and R.W. performed research; A.C., J.W., N.G., Q.Z., and R.W. analyzed data; A.C. and M.P.M. wrote the first draft of the paper; A.C., M.G., and M.P.M. edited the paper; A.C. and M.P.M. wrote the paper; T.M.K. and R.L.V. contributed unpublished reagents/analytic tools.

This work was supported by National Institute on Aging Intramural Research Program.

*A.C. and J.W. contributed equally to this work.

The authors declare no competing financial interests.

Correspondence should be addressed to Aiwu Cheng at chengai@mail.nih.gov or Mark P. Mattson at mmattso2@jhmi.edu.

https://doi.org/10.1523/JNEUROSCI.1446-19.2019

and Zahs, 2010; Driscoll and Troncoso, 2011). During the past three decades, evidence has accumulated from studies of AD patients and experimental models that points to mitochondrial dysfunction and an excitatory imbalance in vulnerable neuronal circuits as early events in AD pathogenesis (Mattson, 2004). For example, PET imaging studies consistently demonstrate impaired cerebral cellular glucose utilization in patients with mild cognitive impairment (MCI) and AD, and fMRI and EEG recording studies have demonstrated an increased incidence of neuronal network hyperexcitability in AD patients compared with controls (Cohen and Klunk, 2014; Kato et al., 2016; Vossel et al., 2016; Lam et al., 2017). Aβ likely contributes to the metabolic impairment and hyperexcitability because aggregating Aβ impairs glucose transport and mitochondrial dysfunction and renders neurons vulnerable to excitotoxicity (Mattson et al., 1992; Mark et al., 1995b, 1997; Keller et al., 1997). Moreover, mouse models of AD that exhibit Aβ plaques and/or tau tangles exhibit associated impairment of cerebral energy metabolism and hyperexcitability of neuronal circuits (Born, 2015; Palop and Mucke, 2016; Reyes-Marin and Nuñez, 2017; Liu et al., 2019).

The core neuronal circuitry throughout the brain is comprised of large excitatory glutamatergic neurons with long axons that often project relatively long distances within and between brain regions, and smaller GABAergic inhibitory interneurons that typically synapse upon adjacent glutamatergic neurons. Perhaps because of their abundance and large size, glutamatergic neurons have been a major focus for studies of neurofibrillary tangle pathology and neuronal loss in AD. However, emerging evidence suggests that GABAergic interneuron dysfunction and degeneration are an early and pivotal event that results in aberrant neuronal circuit hyperexcitability and, consequently, the degeneration of glutamatergic neurons (Palop and Mucke, 2016). Early studies showed that excessive activation of glutamate receptors can cause dendritic atrophy and tau tangle pathology in hippocampal neurons, and GABA receptor agonists can prevent such excitotoxic dendritic damage and neuronal death (Mattson et al., 1988; Mattson and Kater, 1989; Mattson, 1990; Stein-Behrens et al., 1994; Mark et al., 1995a). More recently, it has become clear that interneurons expressing the Ca^{2+}-binding protein parvalbumin (PV) are prone to degeneration in association with Aβ pathology in AD patients and transgenic mouse AD models (Takahashi et al., 2010; Verret et al., 2012).

Mitochondrial dysfunction has been documented in studies of AD patients and AD models (Mattson et al., 2008; Perez Ortiz and Swerdlow, 2019). These mitochondrial abnormalities may result from increased oxidative damage to mitochondrial DNA and proteins and from impaired mitophagy as a result of lysosome dysfunction (Colacurcio and Nixon, 2016; Fang et al., 2019). Because ion-motive ATPases are the major consumer of ATP in active neurons, an impaired ability of mitochondria to generate ATP increases neuronal vulnerability to excitotoxicity (Mattson, 2003; Connolly and Prehn, 2015). The molecular mechanisms that link mitochondrial alterations to PV interneuron degeneration and neuronal circuit hyperexcitability in AD are not known. The NAD^+-dependent protein deacetylase sirtuin 3 (SIRT3) is localized to mitochondria where it acts to remove acetyl groups from lysine residues of hundreds of proteins, including many involved in energy metabolism, oxidative stress mitigation, and membrane permeability regulation (Hafner et al., 2010; Hirschey et al., 2010; Shimazu et al., 2010; Cheng et al., 2016; Carrico et al., 2018). We recently reported that SIRT3 protects neurons against excitotoxic and metabolic stress by mechanisms involving enhanced removal of mitochondrial superoxide and inhibition of apoptosis (Cheng et al., 2016). In the present study, using a model of SIRT3 haploinsufficient AppPs1 mutant transgenic AD mice (Sirt3 $^{+/-}$AppPs1), we gained evidence that reduced levels of SIRT3 led to a significant loss of cerebral cortical interneurons and aggravated neuronal circuit hyperexcitability in AppPs1 mice. These results underscore critical roles for SIRT3 and sustained mitochondria functions in interneuron survival and associated neuronal network activity.

Materials and Methods

Animals. Double-transgenic mice (AppPs1 mice) expressing a chimeric mouse/human amyloid precursor protein (Mo/HuAPP695swe) and a mutant human presenilin 1 (PS1-dE9) in CNS neurons were purchased from the The Jackson Laboratory. Breeding pairs of Sirt3-deficient mice used to establish an in-house colony were a generous gift from David Gius (Northwestern University, Evanston, IL). Both mouse strains were on a congenic C57BL/6J background. The AppPs1 mice were crossbred with Sirt3 $^{-/-}$ mice to generate F1 offspring (Sirt3 $^{+/-}$/AppPs1 or Sirt $^{+/-}$). To expand the colony, Sirt3 $^{+/-}$AppPs1 were crossed with Sirt3 $^{+/-}$ mice or WT mice to get WT, Sirt3 $^{+/-}$, Sirt3 $^{+/-}$AppPs1, AppPs1, Sirt3 $^{-/-}$, and Sirt3 $^{-/-}$AppPs1 littermates. Sirt $^{-/-}$AppPs1 mice were born at very low rates (~6%, lower than the normal Mendelian ratio of 12.5% for crossbreeding of Sirt3 $^{+/-}$AppPs1 with Sirt3 $^{+/-}$); thus, it was difficult to have a large cohort for the investigation. Accordingly, these mice were not used in the study. In addition, Sirt3 $^{+/-}$, not Sirt3 $^{-/-}$ mice, were used in the studies since it was a more relevant control to Sirt3 $^{+/-}$AppPs1 mice. Unless indicated, male mice were used throughout the study for telemetric recording, immunohistology, and biochemical studies in all the genotypes; the numbers of mice used in each experiment are indicated in the figure legends. Methods for genotyping have been described previously (datasheet on AppPs1 mouse strain 005864, The Jackson Laboratory) (Cheng et al., 2016). Mice were provided a standard National Institutes of Health diet (Teklad Global 18% Protein Rodent Diet, Envigo) and were maintained on a 12 h light/dark cycle at 20°C to 22°C. The mice were housed in groups with littermates, except when fed ketone ester (KE) or control diets when they were housed singly. KE (#104404) and control (#1004403) diets were purchased from Dyets. All animal procedures were approved by the Animal Care and Use Committee of the National Institute on Aging Intramural Research Program.

Postmortem tissues and immunoblot analysis. Human postmortem tissues were gifts from the Alzheimer Disease Center, Sanders-Brown Center on Aging (Lexington, KY); detailed information is included in Table 1. To obtain mouse tissues, mice were killed by cervical dislocation at a designated time (either control or with drug administrations), and the cortices were dissected out and quickly put on dry ice. Both human and mouse postmortem tissues were stored in −80°C before processing for immunoblot analysis. For immunoblot analysis, tissues were lysed in RIPA buffer containing protease and phosphatase inhibitors (Millipore Sigma). Lysates were sonicated and centrifuged at 14,000 × *g* for 5 min at 4°C. A final protein concentration of each sample was determined using a protein assay kit (Bio-Rad) with BSA as the standard. Thirty micrograms of protein/lane were resolved in a 4%–10% polyacrylamide gel gradient gel (Invitrogen) and then transferred electrophoretically to a nitrocellulose membrane (Invitrogen). Nonspecific binding sites were blocked in blocking solution containing 5% milk for 2 h at room temperature. Then the membranes were incubated overnight in primary antibodies followed by incubation in secondary antibodies for 1.5 h at room temperature. The reaction products in the membranes were visualized using an enhanced chemiluminescence Western Blot Detection Kit (Thermo Fisher Scientific). Primary antibodies recognized SIRT3 (1:500, Cell Signaling Technology), c-Fos (1:500, Cell Signaling Technology), γH2AX (1:5000, EMD Millipore), and actin (1:1000, Cell Signaling Technology). Secondary antibodies recognizing primary antibodies were HRP-conjugated anti-rabbit or anti-mouse (1:1000; R1006 Kindle Biosciences). The blots were imaged using Kwik-Quant Imager (Kindle Biosciences) using Hi/Lo Digital-ECL Western Blot Detection Kit (R1004; Kindle Biosciences).

Histology and immunohistochemistry. Mice were anesthetized with isoflurane and perfused transcardially with cold PBS, followed by 4% PFA in

Table 1. Clinical data on MCI: AD patients and nondemented control subjects

	Reference #	Age (yr)	Race	Gender	Braak stage	PMI	Brain weight (g)
Controls	1280	86	White	Male	2	4	1125
	1271	71	White	Male	0	2.6	1495
	1268	68	White	Female	1	4	1030
	1260	80	White	Female	1	4.42	1200
	1245	88	White	Male	2	2.17	1290
	1244	90	White	Female	2	2.25	1045
	1221	81	White	Male	2	2.83	1390
	1161	84	White	Female	0	2.5	1230
Mean ± SD		81 ± 7.9			1.3 ± 0.9	3.1 ± 0.9	1225.6 ± 162.8
MCI	1277	78	White	Female	3	3.5	1144
	1225	82	White	Female	5	5	1200
	1164	88	White	Female	3	3	1130
	1122	87	White	Male	4	2.75	1530
	1087	82	White	Female	3	3	1075
	1065	87	White	Male	4	3.5	1200
	1289	92	White	Female	3	2.33	1020
	1152	84	White	Male	4	3.5	1350
Mean ± SD		85 ± 4.4			3.6 ± 0.7	3.3 ± 0.8	1206.1 ± 163.5
AD	1285	88	White	Male	5	1.5	1100
	1202	80	White	Female	6	3.33	1210
	1181	67	White	Female	6	2.25	790
	1160	73	White	Male	6	2	1130
	1144	85	White	Male	6	2.75	1020
	1086	90	White	Female	6	2.75	1090
	1084	86	White	Female	6	3.25	870
	1050	81	White	Male	6	3.75	1040
Mean ± SD		81 ± 7.9			5.9 ± 0.4	2.7 ± 0.8	1031.3 ± 138.5

PBS, pH 7.4. Whole brains were postfixed in 4% PFA in PBS for 2 d and then transferred to 30% sucrose in PBS for cryopreservation at −20°C. Brain sections were cut in the coronal plane at a thickness of 30 μm and collected on Superfrost plus slides (VWR International). For immunostaining, sections were placed in a beaker containing antigen retrieval buffer (10 mM sodium citrate, 0.05% Tween 20, pH 6.0), which was then microwaved until the buffer boiled. Thirty minutes later, the sections were washed in PBS 3 times and then incubated for 1 h in blocking solution (0.3% Triton X-100, 10% normal goat serum) in PBS. Sections were then incubated overnight at 4°C in blocking solution containing primary antibodies. Brain sections were then washed with PBS and incubated with appropriate secondary antibodies diluted in blocking solution for 2 h at room temperature. The brain sections were counterstained with DAPI (0.02% DAPI and 1% RNase in PBS) for 10 min when desired. The primary antibodies used and their dilutions were as follows: rabbit or mouse anti-PV (1:4000, Swant), rabbit anti-calretinin (CR) (1:2000, Swant), rabbit anti-γH2AX (1:200, EMD Millipore), rabbit anti c-Fos (1:200, Cell Signaling Technology), and mouse anti-Aβ (1:500, Biolegend). Secondary antibodies used and their dilutions were fluorescein- or rhodamine-conjugated goat anti-rabbit IgG (1:1000) and fluorescein- or rhodamine-conjugated goat anti-mouse IgG (1:1000) (Vector Laboratories).

TUNEL staining. A TUNEL kit (Trevigen) was used to detect DNA damage. Briefly, the PFA-fixed brain sections were washed with PBS, pH 7.4, and were then permeabilized and preincubated with Cytonin solution (R&D Systems) overnight. After washing with deionized water, the sections were incubated at 37°C for 1 h in a reaction mixture containing terminal transferase, and biotinylated nucleotide or PBS as a control. After immersing with TdT stop buffer and washing in PBS two times for 2–5 min, brain slices were incubated in the presence of streptavidin-fluorescein for 30 min in the dark at room temperature. After rinsing in PBS, DNA strand breakage was visualized by confocal imaging.

Confocal imaging and image analysis. Images of immunostained brain sections were acquired using an Olympus Multiphoton Laser Scanning Microscope with 60× (NA, 1.42), 20× (NA, 0.75), 10× (NA, 0.4), or 4× (NA, 0.16) objectives in dual-scanning mode for simultaneous detection of fluorescein (488 nm excitation and 510 nm emission) and rhodamine (545 nm excitation and 590 nm emission). To quantify GABAergic neuronal loss, the numbers of PV^+ and/or CR^+ immunoreactive neurons were counted in a 500-μm-wide segment through the entire dorsal to ventral extent of the frontal cortex. To acquire images of the full cortical thickness, 2 or 3 images were acquired using a 10× objective (zoom = 1.5) and then montaged using Photoshop (Adobe). Cells were counted in three adjacent sections to determine an average number for each mouse. To quantify TUNEL particle loads, 5–7 images of frontal cortex were acquired from brain sections of each mouse using a 60× or 20× objective. All images were acquired using identical confocal system parameters. $TUNEL^+$ particles were quantified for each image using ImageJ software, and values are expressed as the percentage of the cortical area imaged. The values from 5 to 7 images taken from one brain were averaged to obtain the final value for that animal. Four to six mice of each genotype were used in each experiment, as stated in the figure legends. To analyze γH2AX immunostaining intensity, 8–10 images per mouse of double-label immunofluorescent labeling for γH2AX (green) and PV (red) in the frontal cortex were acquired using identical confocal settings for all brain sections using a 60× objective. Individual PV^+ and surrounding PV^- nuclei in each image were analyzed for fluorescent γH2AX signal intensity. The values from 8 to 10 images taken from one brain were averaged to obtain the final γH2AX intensity of PV^- and PV^+ neurons for that animal. At least 500 total cells and 60 PV^+ cells were analyzed from 4 or 5 mice of each genotype. Images were analyzed using Olympus Fluoview (FV10-ASW2.1) and ImageJ software, and the values are processed using Excel spread sheet. The quantifications were performed by an investigator blinded to the mouse genotype.

Kainic acid (KA) administration, seizure scoring, and mortality rate determination. KA (Abcam) was prepared as a stock solution in PBS at a concentration of 20 mg/ml. Mice were injected intraperitoneally at a single dose of 20 mg/kg (10 μl stock solution /g body weight). Seizure severity was scored using a modified version of the Racine scale (Hamilton et al., 2018). The scale ranged from normal behavior with a score of 0 to death with a score of 6, and with the following intermediate scores: 1, hypoactivity, including crawling, fixed gaze, and/or a hunched postures, with occasional wet-dog shakes; 2, partial clonus: unilateral forelimb clonus, head nodding, frequent wet-dog shakes; 3, mild generalized clonus, rearing, bilateral forelimb clonus, loss of upright posture; 4, severe generalized clonus, falling, and/or uncontrolled running and jumping; 5, status epilepticus with severe loss of balance and tonic limb extension; and 6, seizures culminating in death. Behaviors were scored every 10 min for a period of 2 h after KA administration by a trained experimenter blinded as to the genotype of the mice. After scores for each individual mouse were obtained, mice of same genotype were grouped (8–10 mice per group). The scores at each time point were averaged for that genotype group. In addition to recording seizure scores at each time point, the total seizure severity was determined by integrating individual scores per mouse over the duration of the experiment (2 h or survival time period for each mouse) using the following formula: seizure severity = $\sum$ all scores of a given mice/duration of the scoring period (Giménez-Cassina et al., 2012). The severity score was determined for each mouse, and values for $Sirt3^{+/-}$, AppPs1, and $Sirt3^{+/-}$AppPs1 mice were expressed as a percentage of the average severity score for total WT mice.

KE diet. A KE diet was prepared by Dyets (#104404) using KE (D-β-hydroxybutyrate and (*R*)-1,3-butanediol) produced by two of the authors (T.M.K. and R.L.V.) and an isocaloric control carbohydrate control diet (Dyets, #104403) were formulated as described previously (Kashiwaya et al., 2013). For the control diet, the percentages of kcal derived from carbohydrates, protein, and fat were 65, 24, and 8, respectively. For the KE diet, the percentages of kcal derived from carbohydrates, protein, fat, and β-hydroxybutyrate were 43, 24, 8, and 22, respectively. In addition, both diets contained flavoring (Sugar-Free Jello), which was used to mask the bitterness of the KE.

Telemetric EEG recording. A commercially available telemetry system (Data Sciences International) was used to record the EEG, core body temperature, and general activity (movement in the home cage) mice. A video camera (Swann, NVR87300) was used to record the behavior of each of mice during EEG recording periods. For electrode implantation, mice were anesthetized with isoflurane, and a radio transmitter (ETA-

F10) was surgically implanted intraperitoneally. The transmitter electrodes were passed subcutaneously to the base of the skull. Two burr holes were drilled through the skull at the following coordinates relative to bregma: the positive recording electrode (parietal cortex: AP, −2.0 mm; L, 1.8 mm) and reference electrode (cerebellum: AP, −6.2 mm; L, 2.0 mm); and the electrodes were inserted into the holes above the dura. The electrodes were secured with a tissue adhesive (Loctite 454, Henkel) and dental cement. All procedures were performed using sterile technique, and body temperature was maintained using a heating pad. Immediately after the surgical procedures, each of the mice received extended-release buprenorphine (0.5 mg/kg; ZooPharm). Warm sterile saline (1 ml/mouse) mixed with antibiotics Enrosite (enrofloxacin, 2.5 mg/kg; Norbrook Laboratory) was injected immediately after implantation and twice daily during the next 3 d. The mice were allowed 7–10 d recovery after the implantation, and then EEG activity was recorded continuously for 2 d or 1 week with the mice in their home cages. EEG data were collected using Dataquest ART (DSI, version 4.36) and analyzed offline using NeuroScore software (DSI; version 3.2.0). The EEG signal from artifact-free epochs was subjected to fast Fourier transformation by the algorithm embedded in the Neuroscore software with normalization of spectral calculation. The analysis yielded power spectra between 0 and 100 Hz, and the delta (0.5–4 Hz) and gamma slow (26–50 Hz) bands were specifically analyzed and presented in this study. The seizure-like spikes were identified using the spike detector tool in NeuroScore (DSI, 3.2.0), which can determine individual spikes and spike trains (defined as at least four spikes within a 200 ms time period). A seizure-like spike was defined using the analytic criteria of the minimum value of 100 μV and having a peak amplitude 5× greater than the average baseline value. The occurrence of spikes was assessed in each of the 10 s epochs and summed up in a defined time duration as indicated. To test the antihyperexcitability effect of diazepam (DZP) on Sirt3$^{+/-}$AppPs1 mice, DZP was injected intraperitoneally before 12:00 P.M. at the dosage as indicated. The mouse was returned to its home cage immediately after injection. The recording of EEG and other parameters lasted ~6 h. The recording concluded before the daily light-off schedule (6:30 P.M.) in the colony. The power spectra of EEG data were recorded and analyzed for a period of 6 h after the administration of vehicle (saline) or KA. The reduction of the total number of spikes during the 6 h period was compared with the pre-DZP baseline EEG recording. For the test of the anticonvulsive effect of DZP on KA-induced seizure, DZP injection solution (5 mg/ml; Hospira) was administered intraperitoneally 45 min before KA injection. EEG data were recorded and analyzed for a period of 2 h after the administration of vehicle (saline) or KA.

Statistics. All data are presented as mean ± SEM. The sample size for each experiment is indicated in the figure legends. Statistical analyses were performed using Prism 7.0 software. The data were analyzed by unpaired Student's *t* test or one-way or two-way ANOVA, followed by Student-Newman-Keuls or Bonferroni's *post hoc* tests. In many of the experiments, there are four genotype groups that represent two separate factors: the presence of human AppPs1 and the haploinsufficiency of Sirt3. We also used the factorial two-way ANOVA to answer statistically the main effects and interaction significance. For assessments of survival, Kaplan–Meier survival curves for each group were prepared using GraphPad Prism and two-sided Cox proportional hazards model. Survival data were analyzed by the Cox proportional hazards model to generate hazard ratios (HRs) to the comparison group and their associated *p* values. Statistical significance between subgroups was separately determined by log-rank test. Fisher exact number test was used to compare the seizure incidence; Spearman's ρ test was used to test the correlation. A *p* value <0.05 was considered statistically significant for all the statistics.

Results

SIRT3 levels are reduced in AD patient inferior parietal cortex

To determine whether SIRT3 levels are altered in AD, we performed SIRT3 immunoblot analysis of rapid autopsy (2.7 + 0.8 h postmortem interval) tissue samples from the inferior parietal cortex (a brain region vulnerable to AD pathology) and cerebellum (a relatively unaffected brain region) of 8 AD patients, 8 patients with MCI, and 8 age-matched neurologically normal subjects. Data on the age, gender, postmortem interval, Braak stage, and brain weights are shown in Table 1. We found that SIRT3 protein levels were significantly reduced by ~40% in the inferior parietal cortex (60.83 ± 8.20% of control, $^*p < 0.05$, one-way ANOVA followed by Bonferroni *post hoc* tests), compared with MCI patients (101. 8 ± 11.99% of control) and control subjects (100 ± 10.26%) (Fig. 1), but not in the cerebellum of AD patients (AD: 88.55 ± 7.59%; MCI: 104.7 ± 8.55%; control: 100 ± 10.70%; $p > 0.05$, one-way ANOVA followed by Bonferroni *post hoc* tests).

AppPs1 AD mice with reduced SIRT3 expression exhibit cerebral hyperexcitability, seizures, and early death

To determine whether SIRT3 plays a role in AD pathogenesis, we crossed AppPs1 double-mutant transgenic mice, which develop Aβ plaque deposits and display synaptic dysfunction (Borchelt et al., 1997; Ma et al., 2012), with SIRT3 KO mice (Cheng et al., 2016) to generate AppPs1 mice with reduced SIRT3 levels (Sirt3$^{+/-}$AppPs1 mice). Approximately 60% of the Sirt3$^{+/-}$AppPs1 mice died before the age of 27 weeks (Fig. 2*A*). In contrast, only 25% of AppPs1 mice and <5% of Sirt3$^{+/-}$ and WT mice died during the first 27 weeks of life. Statistically, both AppPs1 and Sirt3$^{+/-}$AppPs1 mice demonstrated significant increase of death rate, compared with WT or Sirt3$^{+/-}$ mice (Fig. 2*A*, $^{**}p < 0.01$, $^{***}p < 0.001$, log-rank test). However, SIRT3 reduction in AppPs1 mice (Sirt3$^{+/-}$AppPs1) further increased the probability of death of AppPs1 mice before the age of 27 weeks (Fig. 2*A*, $^{**}p < 0.01$, log-rank test). Moreover, the survival data were analyzed by Cox proportional hazards model to generate HRs, which are shown in the right table of Figure 2*A*. HR for AppPs1 versus WT and Sirt3$^{+/-}$AppPs1 versus WT were 4.777 and 5.608, respectively, and HR for Sirt3$^{+/-}$AppPs1 versus AppPs1 mice is 2.447, indicating that Sirt3 reduction in AppPs1 mice further increased death probability of AppPs1 mice by 2.447-fold hazard rate. Additionally, we observed that both male and female Sirt3$^{+/-}$/AppPs1 mice died prematurely. There was no gender difference of survival rate in either AppPs1 ($p = 0.7124$, log-rank test) or Sirt3$^{+/-}$AppPs1 mice ($p = 0.4439$, log-rank test) within 27 weeks (Fig. 2-1, available at https://doi.org/10.1523/JNEUROSCI.1446-19.2019.f2-1).

Because several of the Sirt3$^{+/-}$AppPs1 mice exhibited behaviors suggestive of epileptic seizures in the days preceding their deaths, we implanted surface electrodes in the parietal cortex of 3.5-month-old mice of each of the four genotypes and recorded EEG activity telemetrically with the mice in their home cages. We also videotaped mice during EEG recording to enable correlation of behavior with EEG activity. Of the 12 Sirt3$^{+/-}$AppPs1 mice implanted with EEG recording transmitters, 3 died during the 2 week postsurgery recovery period and 2 died during the 1 week EEG recording period, consistent with their high mortality rate (Fig. 2*A*). None of the mice in any of the three other groups died during the postsurgery recovery or EEG recording periods. EEG recordings from WT and Sirt3$^{+/-}$ mice EEG were consistently normal with few or no high-amplitude spikes and no high-frequency bursting activity (Fig. 1*B*). In contrast, AppPs1 and Sirt3$^{+/-}$AppPs1 mice exhibited frequent epileptiform spikes (sharp wave discharges ≥ 5-fold the amplitude of the basal voltage) and moderate to severe epileptiform bursts of activity, respectively (Fig. 2*B*,*C*). Examples of epileptiform spikes are shown in Figure 2*B* (arrowheads), and two Sirt3$^{+/-}$AppPs1 mice that exhibited severe epileptic burst firing episodes are shown in Figure 2*C*, 1 of which died within minutes of intense EEG seizure activity. We quantified total high-amplitude spikes and total ep-

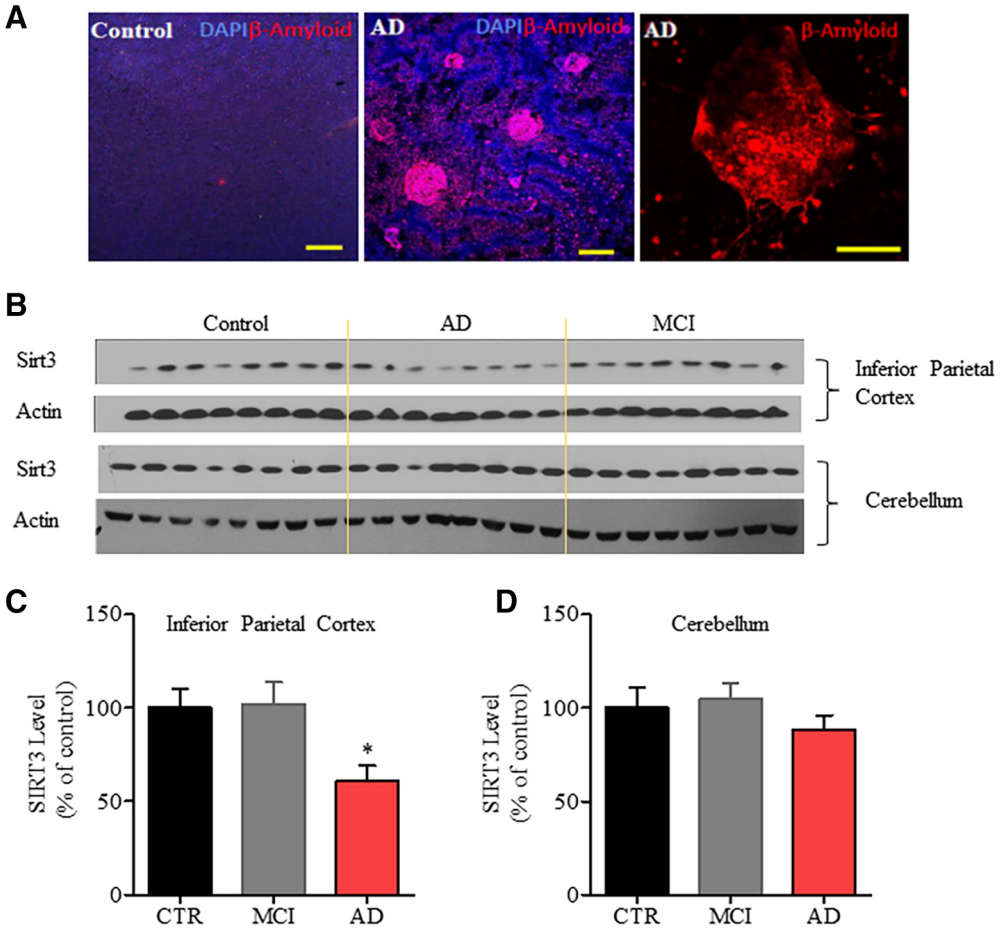

Figure 1. SIRT3 protein levels are reduced in the inferior parietal cortex, but not in the cerebellum, of AD patients. ***A***, Representative images showing Aβ plaques in the inferior parietal cortex of Control and AD patient. Red represents β-amyloid immunostaining. Blue represents DAPI staining. Scale bar, 100 μm. ***B***, Immunoblot analysis of SIRT3 protein levels in samples of inferior parietal cortex (top) and cerebellum (bottom) of 8 neurologically normal control subjects, 8 patients with MCI, and 8 AD patients. ***C***, ***D***, Results of densitometric analysis of SIRT3 protein levels in inferior parietal cortex (***C***) and cerebellum (***D***), normalized to the actin level in the same blot. Values are expressed as a percentage of the SIRT3 level in samples from control subjects (mean ± SEM; $n = 8$ for each group). One-way ANOVA followed by Bonferroni *post hoc* tests: for inferior parietal cortex (***C***), $F_{(2,21)} = 5.079$, $^{*}p = 0.0159$. $^{*}p < 0.05$, comparing Control versus AD or MCI versus AD. For cerebellum (***D***), $F_{(2,21)} = 0.8415$, $p = 0.4451$.

ileptiform bursts over a 24 h period and found no abnormal EEG features in WT and Sirt3$^{+/-}$ mice. AppPs1 mice averaged nearly 300 high-amplitude spikes (288.9 ± 78.19) during a 24 h period, whereas Sirt3$^{+/-}$AppPs1 mice exhibited more than twice the number of high-amplitude spikes (700.1 ± 184.5) (Fig. 2*D*, $t_{(15)} = 1.957$, $^{*}p < 0.05$, unpaired *t* test). The vast majority of Sirt3$^{+/-}$AppPs1 mice (~80% of mice) recorded exhibited bursting activity, whereas AppPs1 mice exhibited occasional bursting activity (~20% of mice). When comparing those mice with epileptiform bursts (excluding the mice without burst firing), the incidences of epileptiform bursts in Sirt3$^{+/-}$AppPs1 (17.5 ± 2.419) were significantly larger than those of AppPs1 (7.75 ± 2.658) (Fig. 2*E*, $t_{(8)} = 2.732$, $^{*}p < 0.05$, unpaired *t* test). Consistently, analysis of video recordings of the mice revealed no behavioral evidence of seizures in WT and Sirt3$^{+/-}$ mice, whereas 25% of AppPs1 mice and 65% of Sirt3$^{+/-}$AppPs1 mice exhibited seizure-related behaviors (Fig. 2*E*) ($^{*}p < 0.05$, Fisher's exact test).

SIRT3 haploinsufficiency sensitizes AppPs1 AD mice to KA-induced seizures and death

Because AppPs1 AD mice with reduced SIRT3 levels exhibit increased spontaneous electrophysiological and behavioral seizures, we determined whether SIRT3 insufficiency affects seizure susceptibility induced by the glutamate receptor agonist KA. Mice of each genotype (15–18 weeks) were administered KA (20 mg/kg, i.p.) and were scored for behavioral manifestations of seizures every 10 min during the ensuing 120 min. During a 2 h observation period after KA injection, WT and Sirt3$^{+/-}$ mice exhibited mild and transient seizures that peaked between 40 and 80 min and then decayed slowly. Seizure severity in WT and Sirt3$^{+/-}$ mice never exceeded a score of 1 (Fig. 3*A*). Seizure scores for AppPs1 mice were significantly greater than WT or Sirt3$^{+/-}$ mice, with many of the AppPs1 mice exhibiting partial clonus and frequent wet-dog shakes. All Sirt3$^{+/-}$AppPs1 mice exhibited severe seizures that consistently manifest as generalized clonus and status epilepticus with seizure scores significantly greater than AppPs1 mice (Fig. 3*A*, $^{*}p < 0.05$, $^{**}p < 0.01$, $^{***}p < 0.001$, two-way ANOVA followed by Bonferroni *post hoc* tests). We also calculated a seizure severity for each mouse in which individual scores of each mouse were summed and integrated over the experimental period. Compared with WT mice (100 ± 23%), AppPs1 (593 ± 131% of WT) and Sirt3$^{+/-}$AppPs1 (1173 ± 102% of WT) mice exhibited ~6-fold and ~12-fold increases in seizure severity, respectively (Fig. 3*B*). Sirt3 insufficiency significantly worsened the seizure severity of AppPs1 mice (Fig. 3*B*, $^{***}p < 0.001$, $^{\#\#\#}p < 0.001$, factorial two-way ANOVA fol-

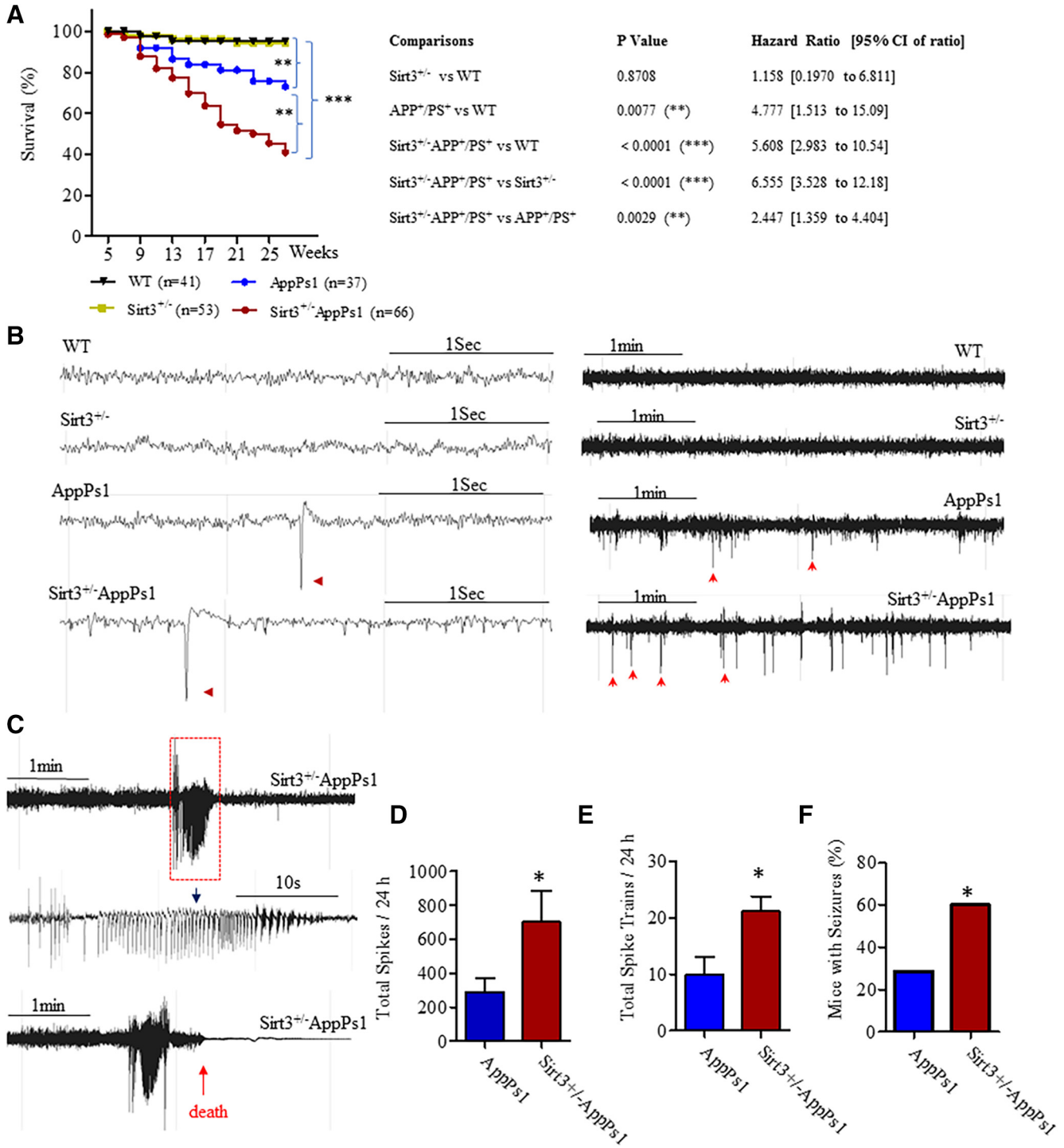

Figure 2. SIRT3 haploinsufficiency triggers cerebral hyperexcitability, seizures, and early death in AppPs1 AD mice. ***A***, Modified Kaplan–Meier survival curves mice of the four indicated genotypes within 27 weeks. WT ($n = 41$: 19 females and 22 males); Sirt3 $^{+/-}$ ($n = 53$: 23 females and 30 males); AppPs1 ($n = 37$, 17 females and 20 males); Sirt3 $^{+/-}$AppPs1 ($n = 66$: 27 females and 39 males). Survival data were analyzed by the Cox proportional hazards model to generate HRs and 95% CI of ratios. The statistical significance of the differences in survival curves was determined by log-rank test. Right, *p* values for the comparisons between different types of mice and their HRs. (See Figure 2-1, available at https://doi.org/10.1523/JNEUROSCI.1446-19.2019.f2-1. There were no gender differences in survival rates for AppPs1 and Sirt3 $^{+/-}$AppPs1 mice within 27 weeks. ***A***, ***B***, Modified Kaplan–Meier survival curves for female and male mice of AppPs1 (***A***) and Sirt3 $^{+/-}$AppPs1 (***B***) mice before the age of 27 weeks. AppPs1 ($n = 7$ females and 20 males); Sirt3 $^{+/-}$AppPs1 ($n = 7$ females and 39 males). The statistical significance between female and male survival curves was determined by log-rank test. Survival data were analyzed by the Cox proportional hazards model to generate HRs and 95% CI of ratios. *p* values and HRs (female vs male) are indicated in the figures. ***B***, Examples of home cage EEG recordings showing high time resolution traces from WT, Sirt3 $^{+/-}$, AppPs1, and Sirt3 $^{+/-}$AppPs1 mice. Calibration: 1 s. Red arrowheads indicate representative large-amplitude single spikes observed in AppPs1 and Sirt3 $^{+/-}$AppPs1 mice, respectively. Following brief high-resolution traces, total 5 min traces from each genotype are shown to illustrate the differences of spike occurrence among them. Calibration: 1 min. Arrows indicate some of representative large-amplitude single spikes. ***C***, EEG recordings showing examples of bursts of epileptiform activity in two Sirt3 $^{+/-}$AppPs1 mice. Bottom, In the case of the EEG recording, the mouse died shortly after the seizure-like activity. ***D***, Quantitative analysis of high-voltage spikes in AppPs1 and Sirt3 $^{+/-}$AppPs1 during a 24 h recording period. Values are mean ± SEM. AppPs1, $n = 8$; Sirt3 $^{+/-}$AppPs1, $n = 9$. *$p = 0.0346$, unpaired *t* test (one-tailed). ***E***, Quantitative analysis of spike trains/bursts during a 24 h recording period in AppPs1 and Sirt3 $^{+/-}$AppPs1. Values are mean ± SEM. AppPs1, $n = 4$; Sirt3 $^{+/-}$AppPs1, $n = 6$. *$p = 0.0129$, unpaired *t* test (one-tailed). ***F***, Percentages of mice exhibiting behavioral manifestations of seizures determined by examination of home cage video recordings. AppPs1 number (seizure vs nonseizure) = 18 (4, 14) and Sirt3 $^{+/-}$AppPs1 (seizure vs nonseizure) = 12 (8, 4). *$p = 0.039$, Fisher exact test (two-sided), and the strength of association: relative risk = 3.0.

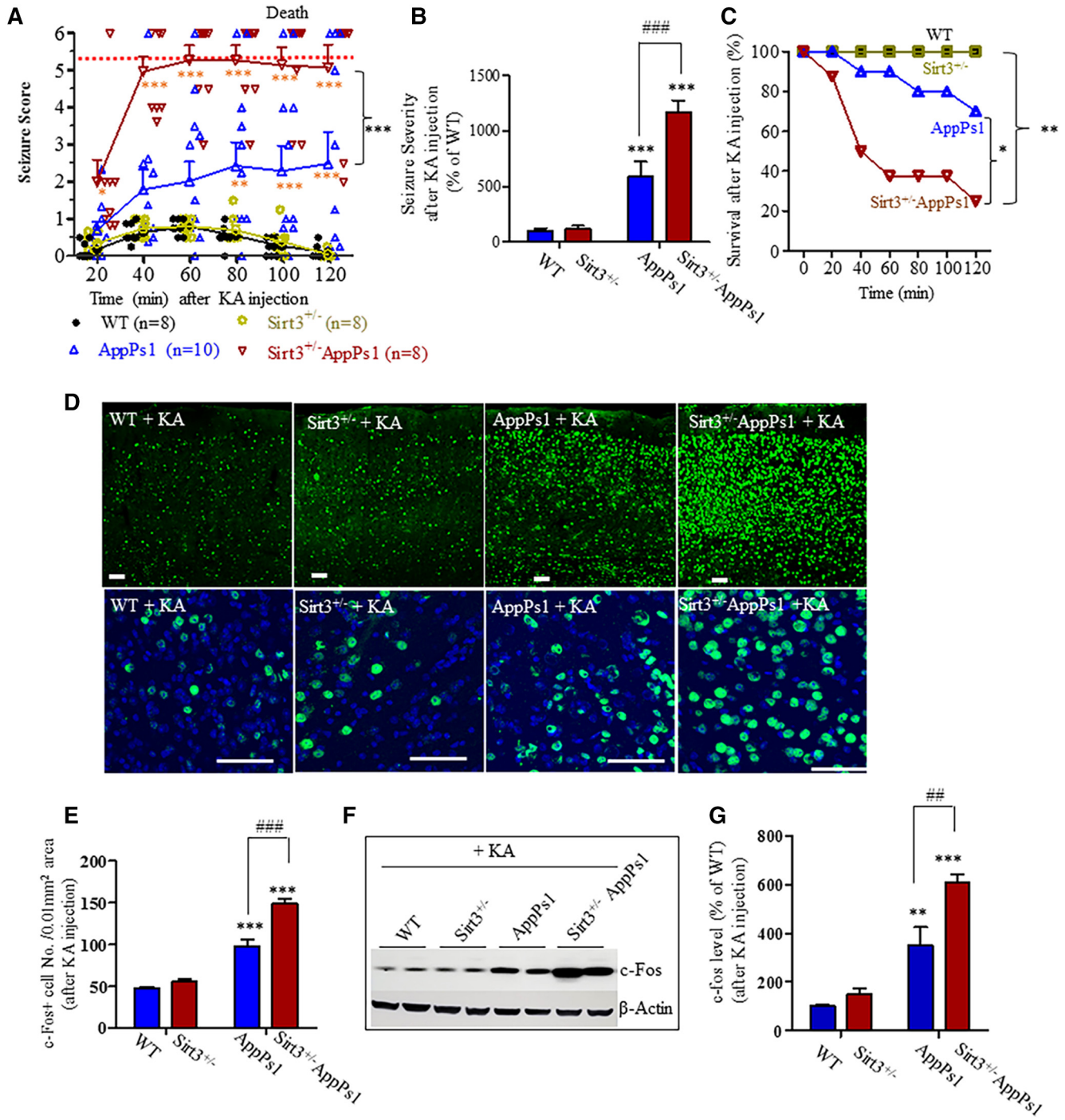

Figure 3. SIRT3 haploinsufficiency sensitizes AppPs1 AD mice to KA-induced seizures and death. ***A***, ***B***, Mice (14 –17 weeks old) were administered KA (20 mg/kg, i.p.), and seizure scores were recorded during 10 min intervals during a 120 min period. ***A***, The average values for every two consecutive 10 min intervals were plotted. ***B***, Overall seizure severity was determined by integrating individual scores per mouse over the duration of the observation period (see Materials and Methods). Values are expressed as a percentage of the value for WT mice (mean ± SEM; 8 –10 mice/group). ***A***, Two-way ANOVA followed by Bonferroni post tests: $F_{group(3,176)} = 127.9$, $^{***}p < 0.001$; $F_{time(5,176)} = 6.6716$, $^{***}p < 0.001$; interaction $^{*}p = 0.017$, $^{*}p < 0.05$, $^{**}p < 0.01$, $^{***}p < 0.001$ versus WT or Sirt3 $^{+/-}$ mice at the corresponding time points. $^{***}p < 0.001$, comparing AppPs1 mice to Sirt3 $^{+/-}$AppPs1 mice at 40, 60, 80, 100, and 120 min time points, respectively. ***B***, Factorial two-way ANOVA (the presence of human AppPs1 and the haploinsufficiency of SIRT3 are considered to be two separate factors) followed by Bonferroni post tests: $F_{sirt3(1,30)} = 10.72$, $^{**}p = 0.0033$; $F_{AppPs1(1,30)} = 68.72$, $^{***}p < 0.0001$; interaction $^{**}p = 0.0052$, $^{***}p < 0.001$ versus WT or Sirt3 $^{+/-}$; $^{###}p < 0.001$, between AppPs1 and Sirt3 $^{+/-}$AppPs1. ***C***, Survival plots for mice of the four genotypes of mice during the 2 h period after KA injection as in Figure 2*A*. WT = 8, Sirt $^{+/-}$ = 8, AppPs1 = 10, and Sirt $^{+/-}$AppPs1 = 8 mice. The statistical significance between survival curves was determined by log-rank test. *p* values for the comparisons between different type of mice and their HRs gained by two-sided Cox proportional hazards model were as follows: Sirt3 $^{+/-}$ versus WT, $p = 1.0$; AppPs1 versus WT or Sirt3 $^{+/-}$, $p = 0.1014$, HR = 6.664; Sirt3 $^{+/-}$AppPs1 versus WT or Sirt3 $^{+/-}$, $^{**}p = 0.0023$, HR = 14.38; Sirt3 $^{+/-}$AppPs1 versus AppPs1, $^{*}p = 0.0361$, HR = 4.786. All the HRs are within 95% CI of ratios. ***D***, Confocal images of c-Fos immunostaining (green) and cell nucleus staining with DAPI (blue) in sections of frontal cortex in mice of the indicated genotypes. Scale bar, 50 μm. ***E***, Numbers of c-Fos $^{+}$ cells per 0.01 mm ^{2} area in sections of the frontal cortex of mice of each genotype. ***F***, Immunoblot analysis of c-Fos levels in frontal cortex of mice 2 h after KA injection. The immunoblots were reprobed with an actin antibody. ***G***, Results of densitometric analysis of immunoblots. Levels of c-Fos were normalized to the level of actin in the same sample. Values are expressed as a percentage of the value for WT mice. ***E***, ***G***, Values are mean ± SEM (4 or 5 mice/group). Factorial two-way ANOVA followed by Bonferroni *post hoc* tests: $F_{sirt3(1,16)} = 28.25$, $^{***}p < 0.0001$; $F_{AppPs1(1,16)} = 164.1$, $^{***}p < 0.0001$; interaction $^{**}p = 0.0014$ for ***E***; and $F_{sirt3(1,12)} = 13.49$, $^{**}p = 0.0037$; $F_{AppPs1(1,12)} = 71.56$, $^{***}p < 0.0001$; interaction $^{*}p = 0.0302$ for ***F***. $^{**}p < 0.01$, $^{***}p < 0.001$ versus WT or Sirt3 $^{+/-}$ mice. $^{##}p < 0.01$, $^{###}p < 0.001$ between AppPs1 and Sirt3 $^{+/-}$AppPs1.

lowed by Bonferroni *post hoc* tests). Moreover, nearly 80% of the Sirt3$^{+/-}$AppPs1 mice died during the 2 h period following KA administration, whereas 30% of the AppPs1 mice died. No WT or Sirt3$^{+/-}$ mice died (Fig. 3*C*, $^{*}p < 0.05$, $^{**}p < 0.01$, log-rank test). The HR data indicated that Sirt3$^{+/-}$AppPs1 were more susceptible to KA-induced seizures and death by 14.38- and 4.786-fold of hazard rate compared with that of WT and AppPS1, respectively (Fig. 3*C*).

At the end of the 2 h period following KA administration, mice were killed and their brains processed for immunohistochemical and immunoblot analysis of c-Fos protein levels. Expression of c-Fos was rapidly induced by the Ca^{2+} influx that occurs in neurons in response to glutamate receptor activation. In WT and Sirt3$^{+/-}$ mice, neurons with intense c-Fos immunoreactivity were relatively sparse in the frontal cortex (Fig. 3*D*, WT: 47.2 ± 2.1/0.01 mm^2 area; Sirt3$^{+/-}$: 55.4 ± 2.9/0.01 mm^2 area). The density of neurons with high c-Fos levels was increased in AppPs1 mice (97.4 ± 8.7/0.01 mm^2 area) and was very high in Sirt3$^{+/-}$ AppPs1 mice (148.9 ± 6.0/0.01 mm^2 area) (Fig. 3*E*, $^{***}p < 0.001$, $^{\#\#\#}p < 0.001$, factorial two-way ANOVA followed by Bonferroni *post hoc* tests). Immunoblot analysis of levels of c-Fos in frontal cortex corroborated the immunohistochemical data as c-Fos levels were significantly greater in AppPs1 mice (349.3 ± 75.22% of WT) compared with WT (100 ± 4.94%) and Sirt3$^{+/-}$ mice (149.5 ± 24.76% of WT) and were significantly greater in Sirt3$^{+/-}$AppPs1 mice (607.6 ± 31.73% of WT) compared with AppPs1 mice (Fig. 3*F*,*G*, $^{**}p < 0.01$, $^{***}p < 0.001$, $^{\#\#}p < 0.01$, factorial two-way ANOVA followed by Bonferroni *post hoc* tests). Collectively, these data indicate that SIRT3 plays critical roles in constraining neural network activity and seizure occurrence and severity in AppPs1 mice.

Reduced SIRT3 expression sensitizes PV-expressing cortical interneurons to KA-induced DNA damage

Degenerating neurons in AD exhibit damage to nuclear DNA, which can be detected *in situ* using the TUNEL staining method and by immunostaining with γ-H2AX antibody, both of which mark double-strand DNA breaks (Adamec et al., 1999; Hou et al., 2018). We processed brain sections from mice that had been killed 2 h after KA administration for TUNEL and γ-H2AX staining and evaluated the cellular localization and amount of staining in the frontal cortex. At this relatively early time point after KA administration, we did not observe neuronal nuclei that exhibited condensed and bright features indicative of apoptosis regardless of mouse genotype. Instead, punctate TUNEL staining was evident at the margins of neuronal nuclei (Fig. 4*A*). We quantified the percentage of TUNEL-stained particles that occupy an area of 10,000 μm^2 and calculated a "TUNEL staining particle load." Compared with WT (0.6488 ± 0.1248) and Sirt3$^{+/-}$ mice (0.7011 ± 0.04576), the TUNEL staining particle load was significantly greater in AppPs1 mice (by ~1.8-fold) (1.232 ± 0.07429) and Sirt3$^{+/-}$AppPs1 mice (2.055 ± 0.2073) (by ~3-fold) (Fig. 4*B*, $^{*}p < 0.05$, $^{***}p < 0.001$, factorial two-way ANOVA followed by Bonferroni *post hoc* tests). Immunoblot analysis showed that γ-H2AX protein levels were significantly greater in AppPs1 mice (443.4 ± 82.49% of WT) (by ~4-fold) and Sirt3$^{+/-}$AppPs1 mice (727.8 ± 100.0% of WT) (by ~7-fold) and were not significantly changed in Sirt3$^{+/-}$ mice (161.4 ± 39.66% of WT) compared with WT (100 ± 13.80%) (Fig. 4*C*,*D*, $^{**}p < 0.01$, factorial two-way ANOVA followed by Bonferroni *post hoc* tests). Both TUNEL staining particle load and γ-H2AX levels were significantly greater in Sirt3$^{+/-}$AppPs1 mice compared with AppPs1 mice (Fig. 4*B*,*D*, $^{\#}p < 0.05$, $^{\#\#}p < 0.01$, factorial two-way ANOVA followed by Bonferroni *post hoc* tests).

PV is expressed in a subpopulation of GABAergic interneurons that exhibit an unusually high spiking frequency (Hu et al., 2014). Evidence from studies of AD patient brain tissue and animal models of AD suggest that GABAergic interneurons, particularly those expressing PV, degenerate early in the disease process (Takahashi et al., 2010; Verret et al., 2012). We next performed double-label immunostaining using antibodies against PV and γ-H2AX after KA administration. Compared with WT (PV$^-$ cells: 100 ± 7.359%; PV$^+$ cells: 114.1 ± 12.1% of WT PV$^-$ cells) and Sirt3$^{+/-}$ mice (PV$^-$ cells: 124.7 ± 9.091% of WT PV$^-$ cells, PV$^+$ cells: 197.5 ± 14.010% of WT PV$^-$ cells), γ-H2AX immunoreactivity in PV$^-$ cortical neurons as well as PV$^+$ interneurons was significantly greater in AppPs1 mice (PV$^-$ cells: 298.0 ± 10.17% of WT PV$^-$ cells, PV$^+$ cells: 335.8 ± 17.38% of WT PV$^-$ cells) and Sirt3$^{+/-}$AppPs1 mice (PV$^-$ cells: 365.8 ± 29.25% of WT PV$^-$ cells, PV$^+$ cells: 798.7 ± 62.97% of WT PV$^-$ cells) (Fig. 4*E*,*F*, $^{***}p < 0.001$, two-way ANOVA followed by Bonferroni *post hoc* tests).

The γ-H2AX immunoreactivities in PV$^-$ and PV$^+$ interneurons were significantly greater in Sirt3$^{+/-}$AppPs1 mice compared with AppPs1 mice (Fig. 4*F*, $^{\#\#\#}p < 0.001$, two-way ANOVA followed by Bonferroni *post hoc* tests). Moreover, PV$^+$ neurons exhibited a higher γH2AX immunofluorescence intensity compared with neurons surrounding them in *Sirt3*$^{+/-}$*AppPs1* mice (Fig. 4*E*). Quantitative analysis of γH2AX immunoreactivity demonstrated significantly higher amounts of γH2AX in PV$^+$ interneurons, compared with other cells, in *Sirt3*$^{+/-}$*AppPs1* and Sirt3$^{+/-}$ mice but not in WT and AppPs1 mice (Fig. 4*E*,*F*, $^{\S\S\S}p < 0.001$, two-way ANOVA followed by *post hoc* unpaired *t* tests). These findings suggest that SIRT3 plays an important role in protecting PV$^+$ interneurons against excitotoxic DNA damage.

SIRT3 haploinsufficiency results in age-dependent loss of PV and CR interneurons in AppPs1 AD mice

Our data to this point demonstrated that SIRT3 reduction aggravated cerebral cortical neuronal networks hyperexcitability in AppPs1 mice and suggested that PV interneurons may be particularly reliant on SIRT3 to protect them against DNA damage. Because Aβ can induce neuronal DNA damage that can trigger cell death (Kruman et al., 2002; Martin, 2008; Sykora et al., 2015), we next counted PV and CR interneuron numbers in the frontal cortex of brain sections from young (4 weeks old) and older mice (4 months old). Examination of the frontal cortex in brain sections that had been double-immunostained with PV and CR antibodies suggested no obvious differences among the four genotypes in 4-week-old mice (Fig. 5*A*,*B*). The results of cell counts showed no significant differences in numbers of PV neurons (in 0.01 mm^2 cortical area, WT: 58.83 ± 3.858; Sirt3$^{+/-}$: 55.68 ± 2.871; AppPs1: 55.78 ± 2.134; Sirt3$^{+/-}$AppPs1: 56.33 ± 5.171) and CR neurons (in 0.01 mm^2 cortical area, WT: 28.13 ± 2.035; Sirt3$^{+/-}$: 28.38 ± 1.44; AppPs1: 27.40 ± 1.065; Sirt3$^{+/-}$AppPs1: 28.88 ± 1.705) among the four genotypes in 4-week-old mice (Fig. 5*D*,*E*, $p > 0.05$, factorial two-way ANOVA followed by Bonferroni *post hoc* tests). In 4-month-old mice, there was a clear reduction in numbers of PV and CR neurons in the Sirt3$^{+/-}$AppPs1 mice compared with each of the other three genotypes (Fig. 5*C*).

The numbers of PV neurons (in 0.01 mm^2 cortical area, WT: 47.36 ± 2.027; Sirt3$^{+/-}$: 40.51 ± 1.610; AppPs1: 39.14 ± 1.507; Sirt3$^{+/-}$AppPs1: 23.76 ± 3.29) and CR neurons (in 0.01 mm^2

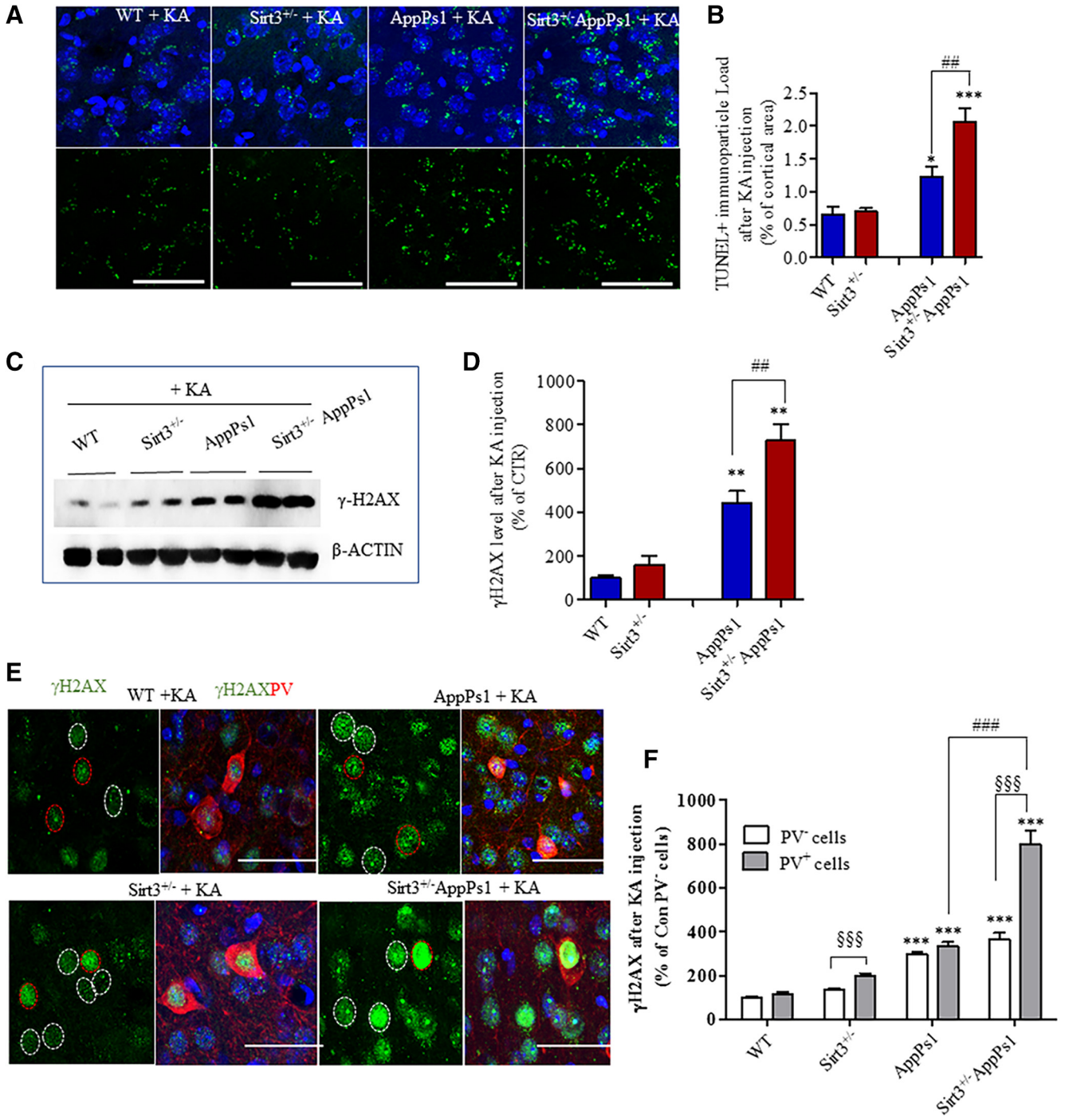

Figure 4. SIRT3 haploinsufficiency sensitizes PV-expressing cortical interneurons to KA-induced DNA damage. Mice (14–17 weeks old) were administered 20 mg/kg KA and 2 h later were either perfused transcardially with 4% PFA (for immunohistochemistry) or fresh cortical tissues were collected for immunoblot analysis. ***A***, Confocal images of TUNEL staining (green) in sections of frontal cortex from mice of the indicated genotypes; sections were counterstained with DAPI to label nuclei (blue). Scale bar, 50 μm. ***B***, TUNEL $^{+}$ particle load expressed as a percentage of the total area of the microscope field. ***C***, Immunoblot of γ-H2AX and actin in samples of frontal cortex from mice of the indicated genotypes. ***D***, Results of densitometric analysis of γ-H2AX levels in frontal cortex of mice of the indicated genotypes. γ-H2AX levels were normalized to the actin level in the same sample. Values are expressed as a percentage of the value for WT mice. ***B***, ***D***, Values are mean ± SEM (4 or 5 mice/group). Factorial two-way ANOVA followed by Bonferroni *post hoc* tests: $F_{sirt3(1,13)} = 9.215$, $^{**}p = 0.0096$; $F_{AppPs1(1,13)} = 45.13$, $^{***}p < 0.0001$; interaction $^{*}p = 0.0192$ for ***B***; and $F_{sirt3(1,14)} = 9.647$, $^{**}p = 0.0077$; $F_{AppPs1(1,14)} = 66.78$, $^{***}p < 0.0001$; interaction $p = 0.0649$ for ***D***. $^{*}p < 0.05$, $^{**}p < 0.01$, $^{***}p < 0.001$ versus WT or Sirt3 $^{+/-}$ mice. $^{\#\#}p < 0.01$ between AppPs1 and Sirt3 $^{+/-}$ AppPs1. ***E***, Confocal images showing γ-H2AX (green) and PV (red) immunoreactivities in frontal cortex sections from mice of the indicated genotypes after KA injection. The sections were counterstained with DAPI (blue). Red circles represent nuclei of PV $^{+}$ neurons. White circles represent nuclei of PV $^{-}$ neurons. ***F***, Quantitative analysis of γ-H2AX immunostaining intensity in all cells (mean) and PV $^{+}$ cells. Values are percentage of the mean value for WT mice. Values are mean ± SEM ($n = 4$ or 5 mice; 15–26 images analyzed/mouse). Two-way ANOVA followed by Bonferroni *post hoc* tests for group and unpaired *t post hoc* tests for cell types: $F_{group(3,26)} = 95.58$, $^{***}p < 0.0001$; $F_{pv\ cells(1,26)} = 40.91$, $^{***}p < 0.0001$; interaction $^{***}p < 0.0001$. $^{***}p < 0.001$ versus WT. $^{\#\#\#}p < 0.001$ between AppPs1 and Sirt3 $^{+/-}$ AppPs1. §§§$p < 0.001$ between PV $^{-}$ and PV $^{+}$ cells.

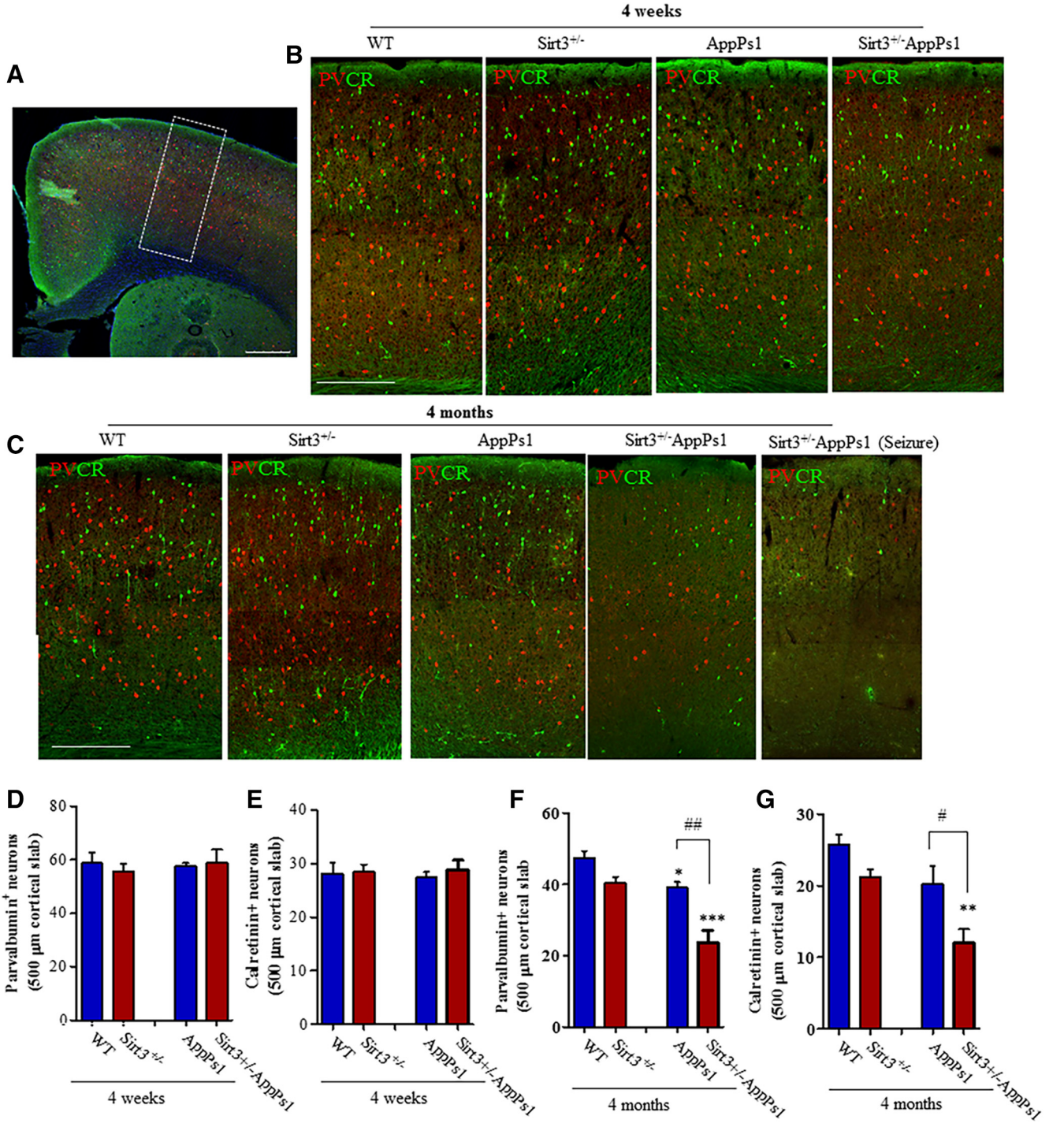

Figure 5. SIRT3 haploinsufficiency triggers loss of PV and CR GABAergic interneurons in AppPs1 AD mice. ***A***, Confocal images showing a coronal section from the frontal cortex of a WT mouse immunostained with PV (red) and CR (green) antibodies. Dotted box represents the region of cortex analyzed. Scale bar, 500 μm. ***B***, Images represent PV and CR immunoreactive neurons in frontal cortex sections from 4-week-old mice of the indicated genotypes. Scale bar, 500 μm. ***C***, Images represent PV and CR immunoreactive neurons in frontal cortex sections from 4-month-old mice of the indicated genotypes. Scale bar, 500 μm. ***D–G***, Graphs represent numbers of PV neurons (***D***, ***F***) and CR neurons (***E***, ***G***) in 4-week-old (***D***, ***E***) and 4-month-old (***F***, ***G***) mice of the indicated genotypes. Values are mean ± SEM (4 – 6 mice/group). Factorial two-way ANOVA followed by Bonferroni *post hoc* tests: $F_{sirt3(1,12)} = 0.1242$, $p = 0.7306$; $F_{AppPs1(1,12)} = 0.1058$, $p = 0.7505$; interaction $p = 0.6251$ for ***D***; $F_{sirt3(1,12)} = 0.2918$, $p = 0.5989$; $F_{AppPs1(1,12)} = 0.005$, $p = 0.9439$; interaction $p = 0.7076$ for ***E***; $F_{sirt3(1,16)} = 25.10$ $^{***}p = 0.0001$, $F_{AppPs1(1,16)} = 31.67$, $^{***}p < 0.0001$, interaction $p = 0.0726$ for ***F***; $F_{sirt3(1,16)} = 17.15$, $^{***}p = 0.0007$; $F_{AppPs1(1,16)} = 17.25$, $^{***}p = 0.0008$; interaction $p = 0.0503$ for ***G***. $^{*}p < 0.05$, $^{**}p < 0.01$, $^{***}p < 0.001$ versus WT or Sirt3 $^{+/-}$. $^{\#}p < 0.05$, $^{\#\#}p < 0.01$ between AppPs1 and *Sirt3* $^{+/-}$ AppPs1. See Figure 5-1 (available at https://doi.org/10.1523/JNEUROSCI.1446-19.2019.f5-1). Loss of GABAergic interneurons in Sirt3 $^{+/-}$/AppPs1 mice in the entorhinal cortex and subiculum. ***A***, Images represent a cerebral hemisphere in a caudal coronal brain section from a 4-month-old WT mouse immunostained with PV (red) and CR (green) antibodies. Yellow and white dotted boxes represent the regions of entorhinal cortex and subiculum, respectively, that were analyzed. ***B***, Images represent PV (red) and CR (green) immunoreactive neurons in entorhinal cortex (top) and subiculum (bottom) of 4-month-old mice of the indicated genotypes. ***C–E***, Graphs represent numbers of PV $^{+}$ cells (***C***, ***E***) and CR $^{+}$ cells (***D***) in 500-μm-wide areas of EC (yellow box area) (***C***, ***D***) and subiculum (***E***) (white box area) of 4-month-old mice of the indicated genotypes. Values are mean and SD ($n = 4 – 6$ mice/group). Factorial two-way ANOVA followed by Bonferroni *post hoc* tests: $F_{sirt3(1,16)} = 4.694$, $^{*}p = 0.0457$; $F_{AppPs1(1,16)} = 8.70$, $^{**}p = 0.0094$; interaction $p = 0.1895$ for ***C***; $F_{sirt3(1,16)} = 8.459$, $^{*}p = 0.0103$; $F_{AppPs1(1,16)} = 11.53$, $^{**}p = 0.0037$; interaction $p = 0.9862$ for ***D***; $F_{sirt3(1,16)} = 17.17$, $^{***}p = 0.0008$; $F_{AppPs1(1,16)} = 66.97$, $^{***}p < 0.0001$; interaction $^{*}p = 0.0163$ for ***E***. $^{*}p < 0.05$, $^{**}p < 0.01$, $^{***}p < 0.001$ versus WT or Sirt3 $^{+/-}$. $^{\#}p < 0.05$, $^{\#\#\#}p < 0.001$ comparing AppPs1 and Sirt3 $^{+/-}$AppPs1.

cortical area, WT: 25.80 ± 1.396; Sirt3$^{+/-}$: 22.29 ± 1.321; AppPs1: 22.27 ± 2.031; Sirt3$^{+/-}$AppPs1: 11.42 ± 1.643) were significantly reduced by >50% in the frontal cortex of Sirt3$^{+/-}$AppPs1 mice compared with mice of each the other three genotypes (Fig. 5*F*,*G*, $^{*}p < 0.05$, $^{**}p < 0.01$, $^{***}p < 0.001$, factorial two-way ANOVA followed by Bonferroni *post hoc* tests). There was a significant reduction (20%) in the numbers of PV neurons in the frontal cortex of AppPs1 mice compared with WT and Sirt3$^{+/-}$ mice, but the reduction was significantly smaller compared with that observed in Sirt3$^{+/-}$AppPs1 mice (Fig. 5*F*, $^{\#}p < 0.05$, $^{\#\#}p < 0.01$ between AppPs1 and *Sirt3*$^{+/-}$*AppPs1*, factorial two-way ANOVA followed by Bonferroni *post hoc* tests). We also found that numbers of PV neurons were significantly reduced in the entorhinal cortex (number of cells in 0.01 mm^2 cortical area, WT: 18.22 ± 1.011; Sirt3$^{+/-}$: 17 ± 1.703; AppPs1: 15.80 ± 2.223; Sirt3$^{+/-}$AppPs1: 10.38 ± 0.706) and subiculum of Sirt3$^{+/-}$AppPs1 mice (number of cells in 0.01 mm^2 cortical area, WT: 30.10 ± 0.666; Sirt3$^{+/-}$: 28.43 ± 0.812; AppPs1: 23.81 ± 1.827; Sirt3$^{+/-}$AppPs1: 16.00 ± 0.7583) compared with mice of each the other three genotypes (Fig. 5-1, available at https://doi.org/10.1523/JNEUROSCI.1446-19.2019.f5-1, $^{*}p < 0.05$, $^{**}p < 0.01$, $^{***}p < 0.001$ vs WT or Sirt3$^{+/-}$, $^{\#}p < 0.05$, $^{\#\#\#}p < 0.001$ comparing AppPs1 and Sirt3$^{+/-}$AppPs1, factorial two-way ANOVA followed by Bonferroni *post hoc* tests).

Pharmacological activation of GABA receptors increases EEG gamma frequency power and suppresses epileptiform activity in SIRT3-deficient AppPs1 AD mice

We next asked whether the hyperexcitability of cortical neuronal networks in Sirt3$^{+/-}$AppPs1 mice could be reversed by treatment with the GABA Type A receptor agonist DZP. We recorded EEGs in Sirt3$^{+/-}$AppPs1 mice before and during a 6 h period after administration of three different doses of DZP (0.15, 0.5, and 2.0 mg/kg). DZP had no significant effect on the power of low-frequency bands (delta, 0.5–4 Hz; theta, 4–8 Hz; α, 8–12 Hz; β, 12–24 Hz; for delta power in Sirt3$^{+/-}$AppPs1 mice, Sal: 2141.68 ± 580.99 μV^2; 0.15 mg DZP: 1792.14 ± 307.95 μV^2; 0.5 mg DZP: 1775.13 ± 541.95 μV^2; 2.0 mg DZP: 1900.93 ± 598.26 μV^2) (Fig. 6*A*, $p > 0.05$, one-way ANOVA with Student-Newman-Keuls *post hoc* tests). Similar to its effects on gamma-slow frequency (26–50 Hz) power in WT mice and human subjects, DZP elicited a dose-dependent increase in gamma-slow frequency power (for gamma-slow power in Sirt3$^{+/-}$AppPs1 mice, Sal: 1486.18 ± 61.80 μV^2; 0.15 mg DZP: 1676.99 ± 100.61 μV^2; 0.5 mg DZP: 2063.56 ± 258.72 μV^2; 2.0 mg DZP: 2504.58 ± 294.36 μV^2) (Fig. 6*B*, $^{*}p < 0.05$, one-way ANOVA with Student-Newman-Keuls *post hoc* tests).

Next, we quantified epileptiform EEG activity in Sirt3$^{+/-}$AppPs1 mice before and during a 6 h period after administration of increasing doses of DZP. DZP dose-dependently reduced the occurrence of high-amplitude spikes (Sal: 100 ± 22.43% of Sal; 0.15 mg DZP: 55.05 ± 6.37% of Sal; 0.5 mg DZP: 15.05 ± 3.03% of Sal; 2.0 mg DZP: 2.57 ± 1.14% of Sal) (Fig. 6*C*, $^{*}p < 0.05$, $^{***}p < 0.0001$, $^{\#}p < 0.05$, one-way ANOVA with Student-Newman-Keuls *post hoc* tests). There was a high correlation between the percentage reduction in high-amplitude spikes and the increase in gamma frequency power (Fig. 6*D*, $^{**}p < 0.01$, Spearman's ρ test). We next administered KA to Sirt3$^{+/-}$AppPs1 mice and recorded EEG before and after exposure to 5 mg/kg DZP. KA-induced epileptiform EEG activity was significantly reduced by DZP (for fraction of time in high-energy spike state, no DZP: 0.511 ± 0.047; with DZP: 0.313 ± 0.022) (Fig. 6*E*,*F*, $t_{(6)} = 3.779$, $^{**}p < 0.01$, unpaired *t* test). Thus, activation of GABA receptors is sufficient to significantly attenuate EEG seizure-related activity in Sirt3$^{+/-}$AppPs1 mice, consistent with a major role for loss of GABAergic interneurons in the neuronal network hyperexcitability in Sirt3$^{+/-}$AppPs1 mice.

Dietary KE induces SIRT3 expression and prevents seizures and death in Sirt3$^{+/-}$AppPs1 AD mice

While DZP can suppress neuronal network hyperexcitability its clinical utility as an intervention for preventing or treating AD is problematic because it can also impair cognition (Foy et al., 1995; Tampellini et al., 2010). It was previously reported that a dietary KE (β-hydroxybutyrate-(*R*)-1,2-butanediol) could ameliorate behavioral deficits pathology in the 3xTgAD mouse model (Kashiwaya et al., 2013). Because the KE is safe and now marketed for human consumption, we designed a study to determine whether the KE diet affects SIRT3 expression and whether the KE diet can preserve GABAergic interneurons in the Sirt3$^{+/-}$AppPs1 mice. Immunoblot analysis of SIRT3 protein levels in cerebral cortical tissue samples of 4-month-old mice revealed the expected significant reduction in SIRT3 levels in Sirt3$^{+/-}$ (56.98 ± 2.79% of WT) and Sirt3$^{+/-}$AppPs1 (30.94 ± 4.28% of WT) mice compared with WT (100 ± 9.04%) and AppPs1 (109.3 ± 7.27% of WT) mice (Fig. 7*A*, $^{***}p < 0.001$, factorial two-way ANOVA followed by Bonferroni *post hoc* tests). In addition, we found that SIRT3 levels were significantly lower in the cerebral cortex of Sirt3$^{+/-}$AppPs1 mice (~70% reduction) compared with Sirt3$^{+/-}$ mice (~50% reduction) (Fig. 7*A*, $^{\#}p < 0.05$, factorial two-way ANOVA).

We then randomly assigned 4-month-old Sirt3$^{+/-}$ mice and Sirt3$^{+/-}$AppPs1 mice to either a control diet or an isocaloric diet containing the KE (for details of diet compositions, see Materials and Methods). After 2 weeks on the diets, levels of SIRT3 in the cerebral cortex were significantly increased in mice on the KE diet compared with mice on the control diet (for Sirt3$^{+/-}$ mice: Ctr, 100 ± 14.67%; KE, 153.5 ± 7.21% of Ctr; for Sirt3$^{+/-}$AppPs1 mice: Ctr, 100 ± 11.28%; KE, 167.3 ± 15.62% of Ctr) (Fig. 7*B*,*C*, $^{**}p < 0.01$, unpaired Student's *t* test).

Next, we randomly assigned 1-month-old Sirt3$^{+/-}$AppPs1 mice to control or KE diets and maintained them on the diets through 24 weeks of age. Whereas 50% of the Sirt3$^{+/-}$AppPs1 mice on the control diet died during this time period, none of the Sirt3$^{+/-}$AppPs1 mice on the KE diet died (Fig. 7*D*, $^{**}p < 0.01$, log-rank test; *HR* (KE/control diet) = 0.2729). We then immunostained brain sections from mice that had been on control or KE diets until 24 weeks of age with PV and CR antibodies and quantified relative densities of these interneurons in the frontal cortex. Sirt3$^{+/-}$AppPs1 mice on the KE diet had significantly greater numbers of both PV (KE: 52.76 ± 1.63) and CR (KE: 22.78 ± 0.80) neurons compared with Sirt3$^{+/-}$AppPs1 mice on the control diet (PV: 30.42 ± 4.84 cells; CR: 15.14 ± 1.91 cells) (Fig. 7*E*, $t_{(7)} = 3.939$ (PV), $t_{(6)} = 3.686$ (CR), $^{**}p < 0.01$, unpaired *t* test, one-tailed). Finally, we administered KA to Sirt3$^{+/-}$AppPs1 mice that had been on control or KE diets from 4 to 24 weeks of age and quantified seizure-related behaviors during the ensuing 2 h. Seizure scores were significantly lower in Sirt3$^{+/-}$AppPs1 mice in the KE group compared with those in the control group (Fig. 7*F*, $^{*}p < 0.05$, $^{***}p < 0.001$ between KE and control food at the corresponding time point, two-way ANOVA followed by Bonferroni post tests).

Discussion

Functional brain imaging studies in humans provide evidence that neuronal network hyperexcitability occurs in vulnerable

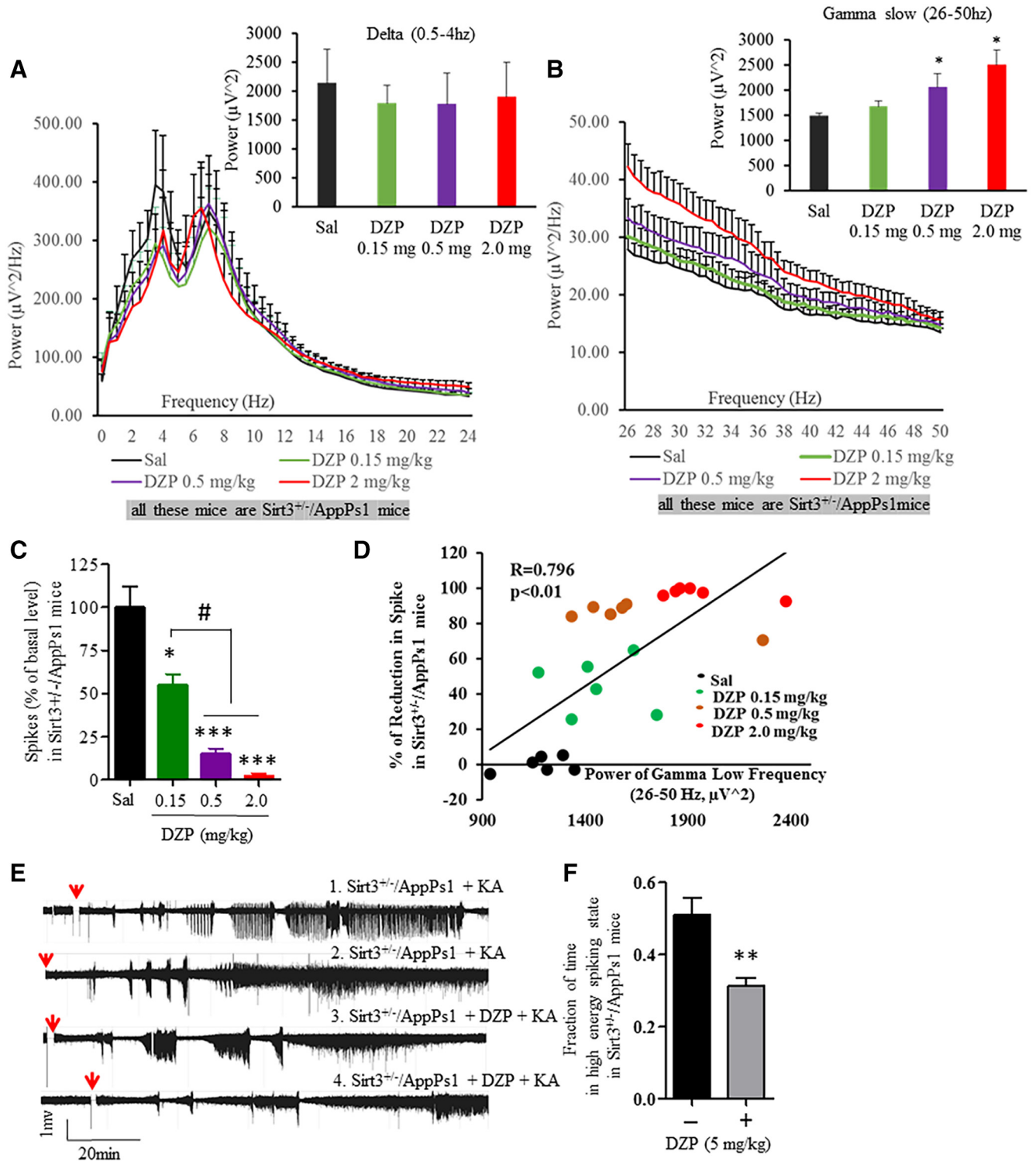

Figure 6. DZP increases gamma frequency power and suppresses epileptiform EEG activity in Sirt3 $^{+/-}$/AppPs1 mice. ***A***, ***B***, EEG power spectra at 0–24 Hz (***A***) and 26–50 Hz (***B***) averaged from a 6 h period after administering the indicated doses of DZP (mg/kg) to Sirt3 $^{+/-}$/AppPs1 mice. Bar graph represents analysis of frequency band powers (***A***, delta band, 0.5–4 Hz; ***B***, gamma slow band, 26–50 Hz). Values are mean ± SEM ($n = 6$ mice). ***C***, Quantitative analysis of high-voltage spikes during a 6 h period after administration of the indicated doses of DZP in Sirt3 $^{+/-}$/AppPs1 mice. Values are expressed as a percentage of the saline-treated value before administration of DZP. Values are mean ± SEM ($n = 6$ mice), One-way ANOVA with Student-Newman-Keuls *post hoc* tests: $F_{(3,20)} = 0.1053$, $p = 0.9560$ for ***A***; $F_{(3,20)} = 12.98$, $^{*}p = 0.0108$ for ***B***; $F_{(3,20)} = 13.98$, $^{***}p < 0.0001$ for ***C***. $^{*}p < 0.05$, $^{***}p < 0.001$ compared with the value for saline-treated control mice. $^{\#}p < 0.05$ between dosages. ***D***, Correlation between the gamma slow band power and the percentage of reduction of high-voltage spikes after administration of the indicated doses of DZP (6 mice). Linear regression. Values are R^2, p, and Spearman's ρ test. ***E***, Examples of EEG recordings in Sirt3 $^{+/-}$/AppPs1 mice beginning 2 h after administration of KA (20 mg/kg). During the recording period, the mice were preadministered either saline or DZP (5 mg/kg) 45 min before KA injections. Red arrows indicate the time of KA injection. ***F***, The fraction of time during the EEG recording period during which high-frequency spiking occurred during a 2 h period after KA administration. Values are mean ± SEM (4 mice/group). $t_{(6)} = 3.779$, $^{**}p = 0.0046$, unpaired t test.

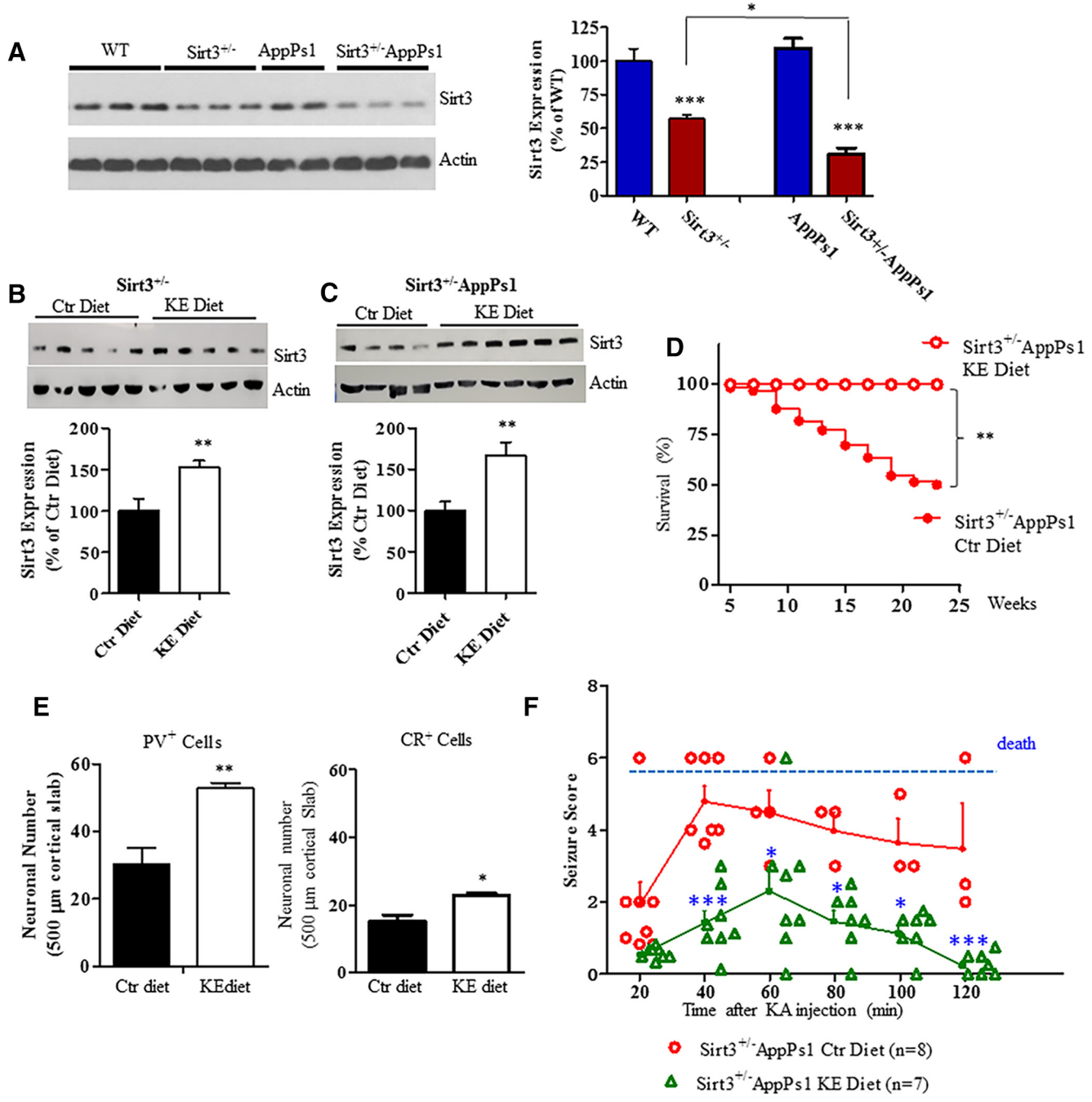

Figure 7. A dietary KE prevents seizures and early death in Sirt3 $^{+/-}$AppPs1 AD mice. ***A***, Immunoblot analysis of SIRT3 protein levels in frontal cortex of 4-month-old WT, SIRT3 $^{+/-}$, AppPs1, and SIRT3 $^{+/-}$/AppPs1 mice (6 or 7 mice per group). Values are mean ± SEM. Factorial two-way ANOVA followed by Bonferroni *post hoc* tests: $F_{sirt3(1,23)} = 98.73$, $^{***}p < 0.0001$; $F_{AppPs1(1,23)} = 1.878$, $p = 0.1838$; interaction $^{**}p = 0.0082$. $^{***}p < 0.001$ versus WT. $^{*}p < 0.05$ between Sirt3 $^{+/-}$ and Sirt3 $^{+/-}$*AppPs1*. ***B***, ***C***, Sirt3 $^{+/-}$ ($n = 10$ mice) and Sirt3 $^{+/-}$/AppPs1 ($n = 10$) mice (4 months old) were fed either a KE-supplemented diet (KE) or a control diet (Ctr) *ad libitum* for 2 weeks. The cortical tissue was removed, and SIRT3 protein levels were determined by immunoblot analysis. Values are mean ± SEM. Unpaired *t* test (one-tailed): $^{**}p < 0.01$. ***D***, Survival plots for Sirt3 $^{+/-}$/AppPs1 mice maintained on either control or KE diets beginning at 1 month of age. Modified Kaplan–Meier survival curves for Sirt3 $^{+/-}$AppPs1 mice under control or KE diets within 23 weeks. Control diets, 66 mice; KE diets, 11 mice. The statistical significance between survival curves was determined by log-rank test. $^{**}p < 0.01$. HR was gained by two-sided Cox proportional hazards model. *HR* (KE/control diet) = 0.2729 (95% CI of ratio: 0.1091–0.6829). ***E***, Results of counts of neurons expressing PV or CR in the frontal cortex of 24-week-old Sirt3 $^{+/-}$/AppPs1 mice that had been maintained on control or KE diets ($n = 4$ or 5 mice/group). Values are mean ± SEM. Unpaired *t* test (one-tailed): $^{**}p < 0.05$, $^{**}p < 0.01$. ***F***, Sirt3 $^{+/-}$ /AppPs1 mice that had been maintained on KE ($n = 7$) or control ($n = 8$) diets from 4 to 24 weeks of age were administered 20 mg/kg KA, and seizure-related behaviors were scored every 10 min during a 2 h time period. The results are plotted as scattered individual points every 20 min and as the mean ± SEM at each time point ($n = 7$ or 8 mice) (solid lines). Two-way ANOVA followed by Bonferroni *post hoc* tests: $F_{group(1,61)} = 73$, $^{***}p < 0.0001$; $F_{time(5,61)} = 6.302$, $^{***}p < 0.0001$; interaction $p = 0.2692$; $^{*}p < 0.05$, $^{***}p < 0.001$ between KE and control food at the corresponding time point.

brain regions early in the disease process and even before cognitive impairment is evident (Putcha et al., 2011; Huijbers et al., 2019). Studies of animal models of AD that exhibit Aβ and/or pTau pathology have consistently demonstrated hyperexcitability of neuronal circuits in the hippocampus and cerebral cortex (Verret et al., 2012; Martinez-Losa et al., 2018). In a prospective study, a cohort of patients with mild AD had a much greater incidence of unprovoked seizures compared with a control pop-

ulation with the greatest increase occurring in AD patients with earlier onset disease (87-fold increase in seizure incidence) (Amatniek et al., 2006). Patients with MCI exhibit hippocampal hyperactivity that can be normalized, and short-term memory improved by acute treatment with a low dose of levetiracetam, an antiepileptic drug that inhibits release of glutamate from presynaptic terminals (Bakker et al., 2012; Vogl et al., 2012). It has been known for >20 years that amyloidogenic APP processing and aggregating Aβ render neurons vulnerable to excitotoxicity (Mattson et al., 1992, 1993) and mitochondrial dysfunction (Keller et al., 1997), but the mechanisms that normally protect neuronal circuits against hyperexcitability in AD are poorly understood. Our findings reveal a critical role for the mitochondrial deacetylase SIRT3 in constraining neuronal circuit excitability in a mouse model of AD. We found that: (1) SIRT3 haploinsufficiency triggers and/or greatly aggravates early-onset seizures and death of AppPs1 double-mutant mice; (2) the neuronal network hyperexcitability in Sirt3$^{+/-}$AppPs1 mice is associated with the loss of PV and CR GABAergic interneurons in the frontal cortex and entorhinal cortex; (3) treating Sirt3$^{+/-}$AppPs1 mice with the GABA receptor agonist DZP enhances gamma frequency EEG power and suppressed seizure activity in Sirt3$^{+/-}$/AppPs1 mice; and (4) a dietary KE increases cerebral cortical SIRT3 expression, prevents loss of PV and CR interneurons, suppresses seizures, and prevents death of Sirt3$^{+/-}$/AppPs1 mice.

Mitochondrial dysfunction in neurons has been suggested to play a role in the pathogenesis of AD, but it is not known which types of neurons are the most vulnerable to mitochondrial dysfunction or how their dysfunction impacts the functional integrity of neuronal circuits. It has been reported that PV interneurons have a very high firing frequency, resulting in a very high-energy and metabolic demand compared with other neurons in the brain (Hu et al., 2014). Moreover, PV interneurons contain exceptionally high amounts of mitochondria compared with other neuronal types in brain (Gulyás et al., 2006), which could meet the high-energy demand for PV neurons under physiological condition. However, under pathological conditions, it renders them particularly vulnerable to compromised mitochondrial function genetically or metabolic and excitotoxic stress during aging and when they encounter Aβ (Kann, 2016). Our previous study (Cheng et al., 2016) showed that mitochondrial SIRT3 deficiency resulted in hyperacetylation of several mitochondrial proteins and compromised mitochondrial functions, leading to a rise in oxidative stress, impaired bioenergetics, unstable mitochondrial membranes, and deficient neuronal Ca^{2+} handling. In the present study, we found that reduced expression of SIRT3 in AppPS1 mice rendered GABAergic interneurons in the cerebral cortex vulnerable to degeneration, causing up to 50% of the PV and CR GABAergic interneurons to be lost at a very young age (4 months old). It also sensitized cortical PV interneurons to acute KA-induced DNA damage. PV interneurons were suggested to be involved in gamma (30–80 Hz) oscillations, which have particular important and interconnected roles in mediating neuronal excitability within cortical microcircuits (Sohal et al., 2009; Hu et al., 2014). Consequently, degeneration of GABAergic interneurons and/or decreased synaptic transmission at GABAergic synapses explains the extreme neural network hyperexcitability in Sirt$^{+/-}$/AppPs1 mice. We found that the GABA Type A receptor agonist DZP increased the gamma slow-band power, correlating significantly with a reduction of epileptiform spikes and bursting firing after KA administration. Previous studies of cultured neurons and synaptosomes showed that aggregating Aβ compromised mitochondrial function and rendered neurons vulnerable to excitotoxicity (Mattson et al., 1992; Mark et al., 1995a, 1997; Keller et al., 1997). The present findings suggest that SIRT3 reduction contributes to the vulnerability of PV and CR interneurons and associated hyperexcitability in Sirt3$^{+/-}$AppPs1 AD mice; conversely, increasing SIRT3 expression might be valuable therapeutically by protecting PV and CR interneurons against Aβ-associated dysfunction and degeneration in AD.

Proteomic analysis of mitochondria from WT and SIRT3 KO cells has identified ~100 proteins that are likely to be regulated by SIRT3 (Rardin et al., 2013; Yang et al., 2016; Carrico et al., 2018). These SIRT3 substrates include mitochondrial electronic transport chain components, the mitochondrial antioxidant enzyme superoxide dismutase 2 (SOD2), mitochondria permeability pore-inducing protein cyclophilin D, fatty acid-β-oxidation, amino acid metabolism, and so on (Hazelton et al., 2009; He et al., 2012; Cheng et al., 2016). SOD2 and cyclophilin D are two mitochondrial proteins that may mediate protection of PV and CR interneurons by SIRT3. SOD2 and cyclophilin D are both deacetylated by SIRT3 in neurons; SOD2 is the major mitochondrial antioxidant enzyme, and its activity is increased by deacetylation, whereas cyclophilin D plays a critical role in triggering mitochondria-mediated apoptosis and its deacetylation is associated with neuroprotection (Cheng et al., 2016). Interestingly, cyclophilin D is highly enriched in PV interneurons (Hazelton et al., 2009), which may explain, at least in part, our finding that PV neurons are highly vulnerable when SIRT3 expression is reduced. Through modification of mitochondrial protein function by deacetylation, SIRT3 can suppress oxidative stress, bolster ATP generation, stabilize mitochondrial membrane potential, and improve neuronal Ca^{2+} handling (Cheng et al., 2016).

A major factor that may render PV and CR interneurons prone to degeneration in AD is the high level of mitochondrial activity required to support their high firing rate. We found that treatment with a KE protects GABAergic interneurons and prevents neuronal network hyperexcitability in Sirt3$^{+/-}$AppPs1 mice, suggesting a potential benefit of the KE or interventions that promote endogenous ketone production in AD. Ketogenic diets are known to suppress seizures in epilepsy patients and a recent clinical trial suggests a potential clinical benefit of ketone precursors (medium chain triglycerides) in AD (Taylor et al., 2018). Our findings suggest that β-hydroxybutyrate, the major ketone produced from fatty acids in ketogenic diets and in response to fasting, can protect GABAergic interneurons against Aβ-induced degeneration by a SIRT3-mediated mechanism. These findings reveal a mitochondria-mediated mechanism that may contribute to the previously reported beneficial effects of KE treatment on cognition and Aβ and pTau pathologies in 3xTgAD mice (Kashiwaya et al., 2013), as well as the ability of the combination of pyruvate and β-hydroxybutyrate to reduce hyperexcitability in AppPs1 mice (Zilberter et al., 2013). Bolstering mitochondrial NAD^+ levels with the NAD^+ precursors nicotinamide and nicotinamide riboside is another approach for enhancing SIRT3 activity and protecting neurons against Aβ and oxidative stress (Liu et al., 2013; Hou et al., 2018; Klimova et al., 2019). Interestingly, exercise and intermittent fasting protect against neuronal dysfunction and cognitive impairment in multiple mouse models of AD and other disorders that involve neuronal excitability (Wang et al., 2005; Halagappa et al., 2007; Nichol et al., 2007; Nigam et al., 2017, Mattson et al., 2018), and also induce expression of SIRT3 in hippocampal and cortical neurons (Cheng et al., 2016; Liu et al., 2019). Moreover, a recent study provided evidence that SIRT3 mediates the upregulation of

GABAergic tone and enhancement of cognition in the hippocampus of mice adapted to an intermittent fasting regimen (Liu et al., 2019). Collectively, emerging evidence suggests that the neuronal network dysfunction that occurs in AD can be reversed by physiological, dietary, and pharmacological interventions to enhance or substitute the functionality of GABAergic interneurons.

References

Adamec E, Vonsattel JP, Nixon RA (1999) DNA strand breaks in Alzheimer's disease. Brain Res 849:67–77.

Amatniek JC, Hauser WA, DelCastillo-Castaneda C, Jacobs DM, Marder K, Bell K, Albert M, Brandt J, Stern Y (2006) Incidence and predictors of seizures in patients with Alzheimer's disease. Epilepsia 47:867–872.

Ashe KH, Zahs KR (2010) Probing the biology of Alzheimer's disease in mice. Neuron 66:631–645.

Bakker A, Krauss GL, Albert MS, Speck CL, Jones LR, Stark CE, Yassa MA, Bassett SS, Shelton AL, Gallagher M (2012) Reduction of hippocampal hyperactivity improves cognition in amnestic mild cognitive impairment. Neuron 74:467–474.

Borchelt DR, Ratovitski T, van Lare J, Lee MK, Gonzales V, Jenkins NA, Copeland NG, Price DL, Sisodia SS (1997) Accelerated amyloid deposition in the brains of transgenic mice coexpressing mutant presenilin 1 and amyloid precursor proteins. Neuron 19:939–945.

Born HA (2015) Seizures in Alzheimer's disease. Neuroscience 286: 251–263.

Carrico C, Meyer JG, He W, Gibson BW, Verdin E (2018) The mitochondrial acylome emerges: proteomics, regulation by sirtuins, and metabolic and misease implications. Cell Metab 27:497–512.

Cheng A, Yang Y, Zhou Y, Maharana C, Lu D, Peng W, Liu Y, Wan R, Marosi K, Misiak M, Bohr VA, Mattson MP (2016) Mitochondrial SIRT3 mediates adaptive responses of neurons to exercise and metabolic and excitatory challenges. Cell Metab 23:128–142.

Cohen AD, Klunk WE (2014) Early detection of Alzheimer's disease using PiB and FDG PET. Neurobiol Dis 72:117–122.

Colacurcio DJ, Nixon RA (2016) Disorders of lysosomal acidification: the emerging role of v-ATPase in aging and neurodegenerative disease. Ageing Res Rev 32:75–88.

Connolly NM, Prehn JH (2015) The metabolic response to excitotoxicity: lessons from single-cell imaging. J Bioenerg Biomembr 47:75–88.

Driscoll I, Troncoso J (2011) Asymptomatic Alzheimer's disease: a prodrome or a state of resilience? Curr Alzheimer Res 8:330–335.

Fang EF, Hou Y, Palikaras K, Adriaanse BA, Kerr JS, Yang B, Lautrup S, Hasan-Olive MM, Caponio D, Dan X, Rocktäschel P, Croteau DL, Akbari M, Greig NH, Fladby T, Nilsen H, Cader MZ, Mattson MP, Tavernarakis N, Bohr VA (2019) Mitophagy inhibits amyloid-beta and tau pathology and reverses cognitive deficits in models of Alzheimer's disease. Nat Neurosci 22:401–412.

Foy A, O'Connell D, Henry D, Kelly J, Cocking S, Halliday J (1995) Benzodiazepine use as a cause of cognitive impairment in elderly hospital inpatients. J Gerontol A Biol Sci Med Sci 50:M990–M106.

Giménez-Cassina A, Martínez-François JR, Fisher JK, Szlyk B, Polak K, Wiwczar J, Tanner GR, Lutas A, Yellen G, Danial NN (2012) BAD dependent regulation of fuel metabolism and K(ATP) channel activity confers resistance to epileptic seizures. Neuron 74:719–730.

Gulyás AI, Buzsáki G, Freund TF, Hirase H (2006) Populations of hippocampal inhibitory neurons express different levels of cytochrome c. Eur J Neurosci 23:2581–2594.

Hafner AV, Dai J, Gomes AP, Xiao CY, Palmeira CM, Rosenzweig A, Sinclair DA (2010) Regulation of the mPTP by SIRT3-mediated deacetylation of CypD at lysine 166 suppresses age-related cardiac hypertrophy. Aging (Albany NY) 2:914–923.

Halagappa VK, Guo Z, Pearson M, Matsuoka Y, Cutler RG, Laferla FM, Mattson MP (2007) Intermittent fasting and caloric restriction ameliorate age-related behavioral deficits in the triple-transgenic mouse model of Alzheimer's disease. Neurobiol Dis 26:212–220.

Hamilton KA, Wang Y, Raefsky SM, Berkowitz S, Spangler R, Suire CN, Camandola S, Lipsky RH, Mattson MP (2018) Mice lacking the transcriptional regulator Bhlhe40 have enhanced neuronal excitability and impaired synaptic plasticity in the hippocampus. PLoS One 13:e0196223.

Hazelton JL, Petrasheuskaya M, Fiskum G, Kristián T (2009) Cyclophilin D is expressed predominantly in mitochondria of gamma-aminobutyric acidergic interneurons. J Neurosci Res 87:1250–1259.

He W, Newman JC, Wang MZ, Ho L, Verdin E (2012) Mitochondrial sirtuins: regulators of protein acylation and metabolism. Trends Endocrinol Metab 23:467–476.

Hirschey MD, Shimazu T, Goetzman E, Jing E, Schwer B, Lombard DB, Grueter CA, Harris C, Biddinger S, Ilkayeva OR, Stevens RD, Li Y, Saha AK, Ruderman NB, Bain JR, Newgard CB, Farese RV Jr, Alt FW, Kahn CR, Verdin E (2010) SIRT3 regulates mitochondrial fatty-acid oxidation by reversible enzyme deacetylation. Nature 464:121–125.

Hou Y, Lautrup S, Cordonnier S, Wang Y, Croteau DL, Zavala E, Zhang Y, Moritoh K, O'Connell JF, Baptiste BA, Stevnsner TV, Mattson MP, Bohr VA (2018) NAD(+) supplementation normalizes key Alzheimer's features and DNA damage responses in a new AD mouse model with introduced DNA repair deficiency. Proc Natl Acad Sci U S A 115: E1876–E1885.

Hu H, Gan J, Jonas P (2014) Interneurons: fast-spiking, parvalbumin(+) GABAergic interneurons: from cellular design to microcircuit function. Science 345:1255263.

Huijbers W, Schultz AP, Papp KV, LaPoint MR, Hanseeuw B, Chhatwal JP, Hedden T, Johnson KA, Sperling RA (2019) Tau accumulation in clinically normal older adults is associated with hippocampal hyperactivity. J Neurosci 39:548–556.

Kann O (2016) The interneuron energy hypothesis: implications for brain disease. Neurobiol Dis 90:75–85.

Kashiwaya Y, Bergman C, Lee JH, Wan R, King MT, Mughal MR, Okun E, Clarke K, Mattson MP, Veech RL (2013) A ketone ester diet exhibits anxiolytic and cognition-sparing properties, and lessens amyloid and tau pathologies in a mouse model of Alzheimer's disease. Neurobiol Aging 34:1530–1539.

Kato T, Inui Y, Nakamura A, Ito K (2016) Brain fluorodeoxyglucose (FDG) PET in dementia. Ageing Res Rev 30:73–84.

Keller JN, Pang Z, Geddes JW, Begley JG, Germeyer A, Waeg G, Mattson MP (1997) Impairment of glucose and glutamate transport and induction of mitochondrial oxidative stress and dysfunction in synaptosomes by amyloid beta-peptide: role of the lipid peroxidation product 4-hydroxynonenal. J Neurochem 69:273–284.

Klimova N, Long A, Kristian T (2019) Nicotinamide mononucleotide alters mitochondrial dynamics by SIRT3-dependent mechanism in male mice. J Neurosci Res 97:975–990.

Kruman II, Kumaravel TS, Lohani A, Pedersen WA, Cutler RG, Kruman Y, Haughey N, Lee J, Evans M, Mattson MP (2002) Folic acid deficiency and homocysteine impair DNA repair in hippocampal neurons and sensitize them to amyloid toxicity in experimental models of Alzheimer's disease. J Neurosci 22:1752–1762.

Lam AD, Deck G, Goldman A, Eskandar EN, Noebels J, Cole AJ (2017) Silent hippocampal seizures and spikes identified by foramen ovale electrodes in Alzheimer's disease. Nat Med 23:678–680.

Liu D, Pitta M, Jiang H, Lee JH, Zhang G, Chen X, Kawamoto EM, Mattson MP (2013) Nicotinamide forestalls pathology and cognitive decline in Alzheimer mice: evidence for improved neuronal bioenergetics and autophagy procession. Neurobiol Aging 34:1564–1580.

Liu Y, Cheng A, Li YJ, Yang Y, Kishimoto Y, Zhang S, Wang Y, Wan R, Raefsky SM, Lu D, Saito T, Saido T, Zhu J, Wu LJ, Mattson MP (2019) SIRT3 mediates hippocampal synaptic adaptations to intermittent fasting and ameliorates deficits in APP mutant mice. Nat Commun 10:1886–1896.

Ma T, Du X, Pick JE, Sui G, Brownlee M, Klann E (2012) Glucagon-like peptide-1 cleavage product GLP-1(9–36) amide rescues synaptic plasticity and memory deficits in Alzheimer's disease model mice. J Neurosci 32:13701–13708.

Mark RJ, Ashford JW, Goodman Y, Mattson MP (1995a) Anticonvulsants attenuate amyloid beta-peptide neurotoxicity, Ca^{2+} deregulation, and cytoskeletal pathology. Neurobiol Aging 16:187–198.

Mark RJ, Hensley K, Butterfield DA, Mattson MP (1995b) Amyloid beta-peptide impairs ion-motive ATPase activities: evidence for a role in loss of neuronal Ca^{2+} homeostasis and cell death. J Neurosci 15:6239–6249.

Mark RJ, Pang Z, Geddes JW, Uchida K, Mattson MP (1997) Amyloid beta-peptide impairs glucose transport in hippocampal and cortical neurons: involvement of membrane lipid peroxidation. J Neurosci 17:1046–1054.

Martin LJ (2008) DNA damage and repair: relevance to mechanisms of neurodegeneration. J Neuropathol Exp Neurol 67:377–387.

Martinez-Losa M, Tracy TE, Ma K, Verret L, Clemente-Perez A, Khan AS, Cobos I, Ho K, Gan L, Mucke L, Alvarez-Dolado M, Palop JJ (2018) Nav1.1-overexpressing interneuron transplants restore brain rhythms

and cognition in a mouse model of Alzheimer's disease. Neuron 98:75–89.e5.
Mattson MP (1990) Antigenic changes similar to those seen in neurofibrillary tangles are elicited by glutamate and Ca^{2+} influx in cultured hippocampal neurons. Neuron 4:105–117.
Mattson MP (2003) Excitotoxic and excitoprotective mechanisms: abundant targets for the prevention and treatment of neurodegenerative disorders. Neuromolecular Med 3:65–94.
Mattson MP (2004) Pathways towards and away from Alzheimer's disease. Nature 430:631–639.
Mattson MP, Kater SB (1989) Excitatory and inhibitory neurotransmitters in the generation and degeneration of hippocampal neuroarchitecture. Brain Res 478:337–348.
Mattson MP, Dou P, Kater SB (1988) Outgrowth-regulating actions of glutamate in isolated hippocampal pyramidal neurons. J Neurosci 8:2087–2100.
Mattson MP, Cheng B, Davis D, Bryant K, Lieberburg I, Rydel RE (1992) Beta-amyloid peptides destabilize calcium homeostasis and render human cortical neurons vulnerable to excitotoxicity. J Neurosci 12:376–389.
Mattson MP, Cheng B, Culwell AR, Esch FS, Lieberburg I, Rydel RE (1993) Evidence for excitoprotective and intraneuronal calcium-regulating roles for secreted forms of the beta-amyloid precursor protein. Neuron 10:243–254.
Mattson MP, Gleichmann M, Cheng A (2008) Mitochondria in neuroplasticity and neurological disorders. Neuron 60:748–766.
Mattson MP, Moehl K, Ghena N, Schmaedick M, Cheng A (2018) Intermittent metabolic switching, neuroplasticity and brain health. Nat Rev Neurosci 19:63–80.
Nichol KE, Parachikova AI, Cotman CW (2007) Three weeks of running wheel exposure improves cognitive performance in the aged Tg2576 mouse. Behav Brain Res 184:124–132.
Nigam SM, Xu S, Kritikou JS, Marosi K, Brodin L, Mattson MP (2017) Exercise and BDNF reduce abeta production by enhancing alpha-secretase processing of APP. J Neurochem 142:286–296.
Palop JJ, Mucke L (2016) Network abnormalities and interneuron dysfunction in Alzheimer disease. Nat Rev Neurosci 17:777–792.
Perez Ortiz JM, Swerdlow RH (2019) Mitochondrial dysfunction in Alzheimer's disease: role in pathogenesis and novel therapeutic opportunities. Br J Pharmacol 176:3489–3507.
Putcha D, Brickhouse M, O'Keefe K, Sullivan C, Rentz D, Marshall G, Dickerson B, Sperling R (2011) Hippocampal hyperactivation associated with cortical thinning in Alzheimer's disease signature regions in non-demented elderly adults. J Neurosci 31:17680–17688.
Rardin MJ, Newman JC, Held JM, Cusack MP, Sorensen DJ, Li B, Schilling B, Mooney SD, Kahn CR, Verdin E, Gibson BW (2013) Label-free quantitative proteomics of the lysine acetylome in mitochondria identifies substrates of SIRT3 in metabolic pathways. Proc Natl Acad Sci U S A 110:6601–6606.
Reyes-Marin KE, Nuñez A (2017) Seizure susceptibility in the APP/PS1 mouse model of Alzheimer's disease and relationship with amyloid beta plaques. Brain Res 1677:93–100.
Shimazu T, Hirschey MD, Hua L, Dittenhafer-Reed KE, Schwer B, Lombard DB, Li Y, Bunkenborg J, Alt FW, Denu JM, Jacobson MP, Verdin E (2010) SIRT3 deacetylates mitochondrial 3-hydroxy-3-methylglutaryl CoA synthase 2 and regulates ketone body production. Cell Metab 12:654–661.
Sohal VS, Zhang F, Yizhar O, Deisseroth K (2009) Parvalbumin neurons and gamma rhythms enhance cortical circuit performance. Nature 459:698–702.
Stein-Behrens B, Mattson MP, Chang I, Yeh M, Sapolsky R (1994) Stress exacerbates neuron loss and cytoskeletal pathology in the hippocampus. J Neurosci 14:5373–5380.
Sykora P, Misiak M, Wang Y, Ghosh S, Leandro GS, Liu D, Tian J, Baptiste BA, Cong WN, Brenerman BM, Fang E, Becker KG, Hamilton RJ, Chigurupati S, Zhang Y, Egan JM, Croteau DL, Wilson DM 3rd, Mattson MP, Bohr VA (2015) DNA polymerase beta deficiency leads to neurodegeneration and exacerbates Alzheimer disease phenotypes. Nucleic Acids Res 43:943–959.
Takahashi H, Brasnjevic I, Rutten BP, Van Der Kolk N, Perl DP, Bouras C, Steinbusch HW, Schmitz C, Hof PR, Dickstein DL (2010) Hippocampal interneuron loss in an APP/PS1 double-mutant mouse and in Alzheimer's disease. Brain Struct Funct 214:145–160.
Tampellini D, Capetillo-Zarate E, Dumont M, Huang Z, Yu F, Lin MT, Gouras GK (2010) Effects of synaptic modulation on beta-amyloid, synaptophysin, and memory performance in Alzheimer's disease transgenic mice. J Neurosci 30:14299–14304.
Taylor MK, Sullivan DK, Mahnken JD, Burns JM, Swerdlow RH (2018) Feasibility and efficacy data from a ketogenic diet intervention in Alzheimer's disease. Alzheimers Dement (N Y) 4:28–36.
Verret L, Mann EO, Hang GB, Barth AM, Cobos I, Ho K, Devidze N, Masliah E, Kreitzer AC, Mody I, Mucke L, Palop JJ (2012) Inhibitory interneuron deficit links altered network activity and cognitive dysfunction in Alzheimer model. Cell 149:708–721.
Vogl C, Mochida S, Wolff C, Whalley BJ, Stephens GJ (2012) The synaptic vesicle glycoprotein 2A ligand levetiracetam inhibits presynaptic Ca^{2+} channels through an intracellular pathway. Mol Pharmacol 82:199–208.
Vossel KA, Ranasinghe KG, Beagle AJ, Mizuiri D, Honma SM, Dowling AF, Darwish SM, Van Berlo V, Barnes DE, Mantle M, Karydas AM, Coppola G, Roberson ED, Miller BL, Garcia PA, Kirsch HE, Mucke L, Nagarajan SS (2016) Incidence and impact of subclinical epileptiform activity in Alzheimer's disease. Ann Neurol 80:858–870.
Wang J, Ho L, Qin W, Rocher AB, Seror I, Humala N, Maniar K, Dolios G, Wang R, Hof PR, Pasinetti GM (2005) Caloric restriction attenuates beta-amyloid neuropathology in a mouse model of Alzheimer's disease. FASEB J 19:659–661.
Yang W, Nagasawa K, Münch C, Xu Y, Satterstrom K, Jeong S, Hayes SD, Jedrychowski MP, Vyas FS, Zaganjor E, Guarani V, Ringel AE, Gygi SP, Harper JW, Haigis MC (2016) Mitochondrial Sirtuin Network Reveals Dynamic SIRT3-Dependent Deacetylation in Response to Membrane Depolarization. Cell 167: 985–1000.e21.
Zilberter M, Ivanov A, Ziyatdinova S, Mukhtarov M, Malkov A, Alpár A, Tortoriello G, Botting CH, Fülöp L, Osypov AA, Pitkänen A, Tanila H, Harkany T, Zilberter Y (2013) Dietary energy substrates reverse early neuronal hyperactivity in a mouse model of Alzheimer's disease. J Neurochem 125:157–171.